Chapter 11

Thermal Methods

Thermal methods, particularly steamdrive and steam soak, are the most successful enhanced-oil-recovery (EOR) processes. They are certainly the most mature. In Chapter 1, we saw that steam methods currently account for approximately one-half the EOR in the United States. Thermal flooding is commercially successful and has been for almost 50 years. In this chapter, we explore the reasons for this success.

Despite the success—billions of barrels have been recovered by this type of EOR—even more hard-to-recover oil remains. Meyer and Attanasi (2003) report that recoverable heavy oil and bitumen resources are almost 1,000 billion barrels, or approximately twice the amount of recoverable light oil. Much of this target is beyond the limits of current technology; hence, thermal methods are constantly evolving to meet these challenges. This chapter touches on these new technologies.

We can give no more than an overview of these scientifically interesting and complex processes. Several texts (White and Moss 1983; Burger et al. 1985; Boberg 1988; Butler 1997) and a monograph (Prats 1982) are available on thermal flooding alone. There are also extensive treatments in reservoir-engineering texts (Gates 2011). Our intent is to apply the twin bases of this text—phase behavior and fractional-flow theory—to thermal methods in some detail. In addition, we deal with the important ancillary topic of heat loss.

This chapter is organized differently from the others, partly because of the many different processes available. We begin with a discussion of viscosity reduction, followed by an overview of the various processes. The bulk of the chapter focuses on mass and

heat transfer specifically directed to thermal methods. This section could constitute a treatment of heat transfer in general because virtually every form of energy transfer occurs in thermal processes. The chapter concludes by returning to discuss the specific processes.

Thermal methods rely on several displacement mechanisms to recover oil, but the most important is the reduction of crude viscosity with increasing temperature. We can draw several important conclusions from **Fig. 11.1**, a plot of crude kinematic viscosity ($\nu_2 = \mu_2/\rho_2$) vs. temperature.

Crude kinematic viscosity decreases dramatically with a rise in temperature. This effect reflects principally the change in dynamic viscosity μ_2 because crude density changes relatively little with temperature. For example, a heavy crude (10–20° API) that undergoes a temperature increase from 300 to 400 K, which is easily obtainable by thermal methods, will produce a viscosity well within the flowing range (less than 10 mPa·s). (The previous sentence begins a practice of using the words *light* and *heavy* for nonviscous and viscous fluids, even though light and heavy, strictly speaking, refer to density. Because there usually exists a correlation between viscosity and density and the usage is thoroughly ingrained, the authors hope that there is no confusion.) Fig. 11.1 greatly compresses the vertical axis simply to plot the observed changes on one scale.

For lighter crudes, the viscosity reduction is less. Therefore, thermal methods are not nearly as advantageous for these crudes, particularly because waterflooding would probably be an attractive alter-native. The viscosity reduction for very heavy crudes (less than 10° API) is substantial, but still not enough to make them flow economically. Therefore, there are practical limits on both viscosity extremes.

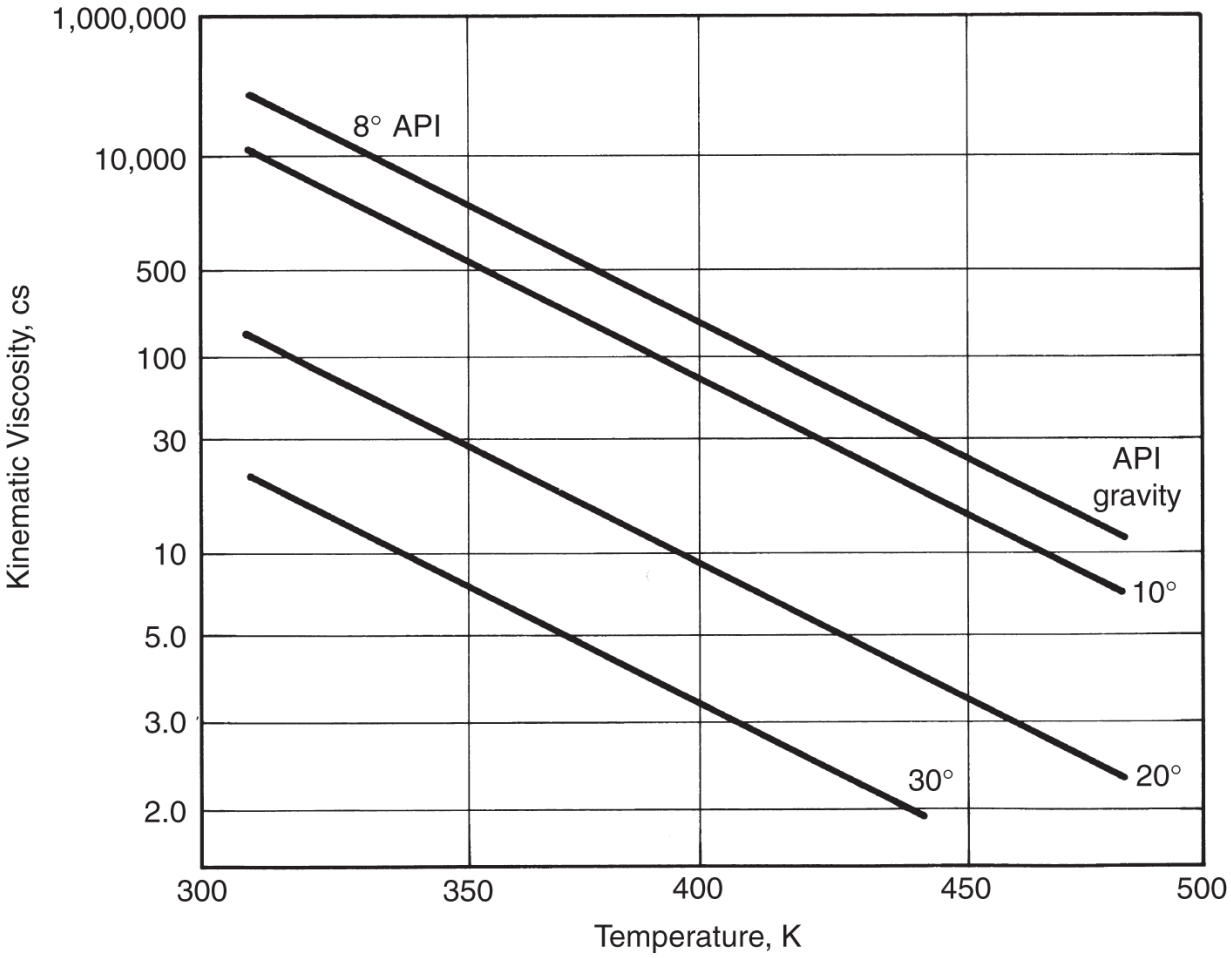

Fig. 11.1—Effect of temperature on crude-oil viscosity [adapted from Farouq Ali (1974)].

11.1 Process Variations

All thermal-recovery processes move or transport energy (usually heat) into or through a reservoir to recover crude. The basic heat-transfer mechanisms are:

Convection. Convection is the transfer of heat by a moving fluid. When the flow is caused by potential (pressure) differences, the convection is said to be *forced*. If it is caused by density differences induced by temperature changes, it is *free* convection. Convection is normally the most important heat-transfer mechanism.

Conduction. Conduction occurs in the absence of fluid movement (e.g., through a tube wall) in the solid portion of a

reservoir, or to adjacent strata. It is heat transfer on a molecular level.

Radiation. Radiation is heat transfer that occurs in a nonmaterial or *photon* phase (Bird et al. 2002). Radiation can occur in the absence of a material phase, either solid or liquid, or it can occur with flow of a material phase, in which case some of the radiation is adsorbed into the material phase, raising its temperature

There are many ways to introduce heat into a reservoir. Most of these involve introducing steam.

Steam Soak. In a steam soak (also known as a cyclic stimulation or huff-n-puff), steam is introduced into a well, and then the well is returned to production after a brief shut-in period **(Fig. 11.2a).** The steam heats up a zone near the well and also provides some pressure support for subsequent production. The shut-in or soak period enables thermal gradients to equalize, but should not be long enough for the pressure to escape. During shut-in, all the injected steam condenses, and the well produces a mixture of hot water and oil. One great advantage of a steam soak is that all the wells can be producing nearly all the time, the injection and soak periods usually being short.

Steamdrive. A steamdrive uses at least two sets of wells, those into which steam is injected and those from which oil is produced (Fig. 11.2b). A steamdrive usually results in higher ultimate recoveries than a steam soak because it penetrates more deeply into the reservoir than steam soaks. For the same reason, well spacing need not be as close in drives as in soaks for equivalent oil recovery. The close spacing partially offsets the disadvantage of sacrificing some of the wells to injection. Because steamdrive is present to some extent in all thermal processes, we will focus on it in later analyses.

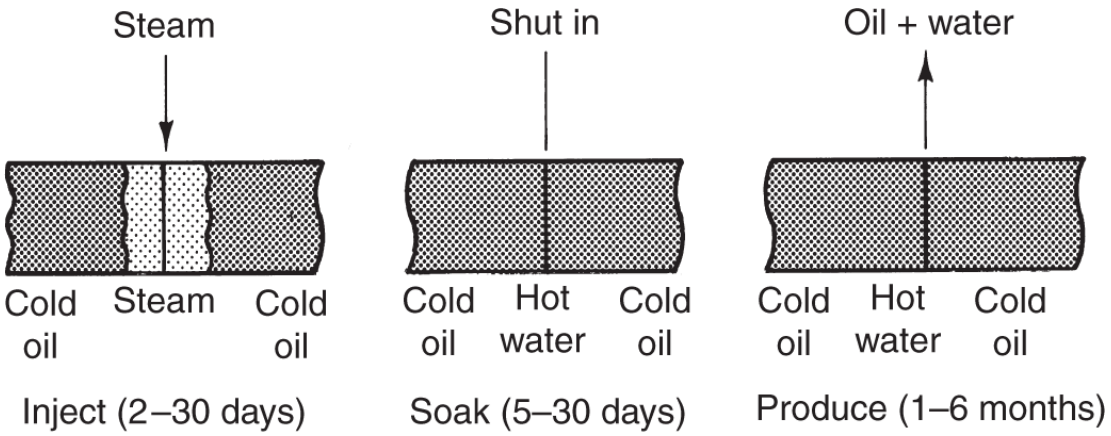

(a) Steam soak or huff-n-puff

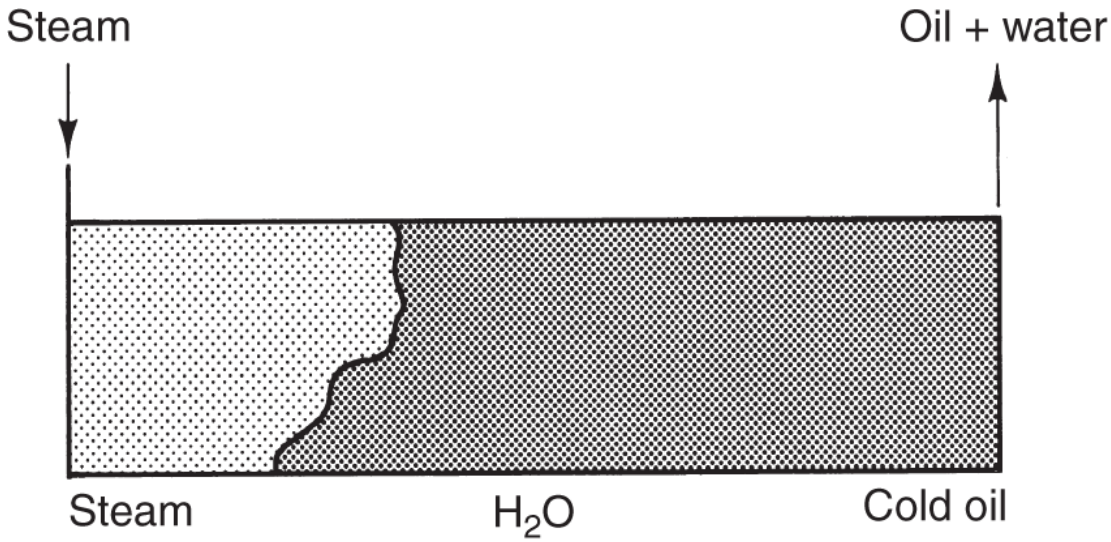

(b) Steamdrive

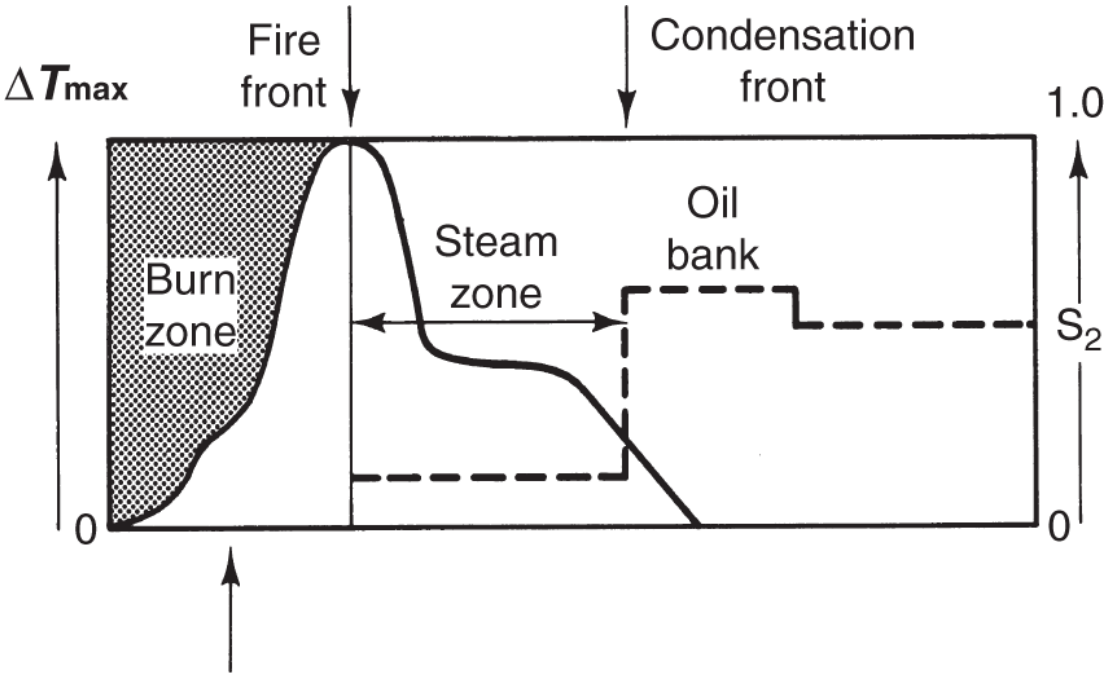

(c) In-situ combustion

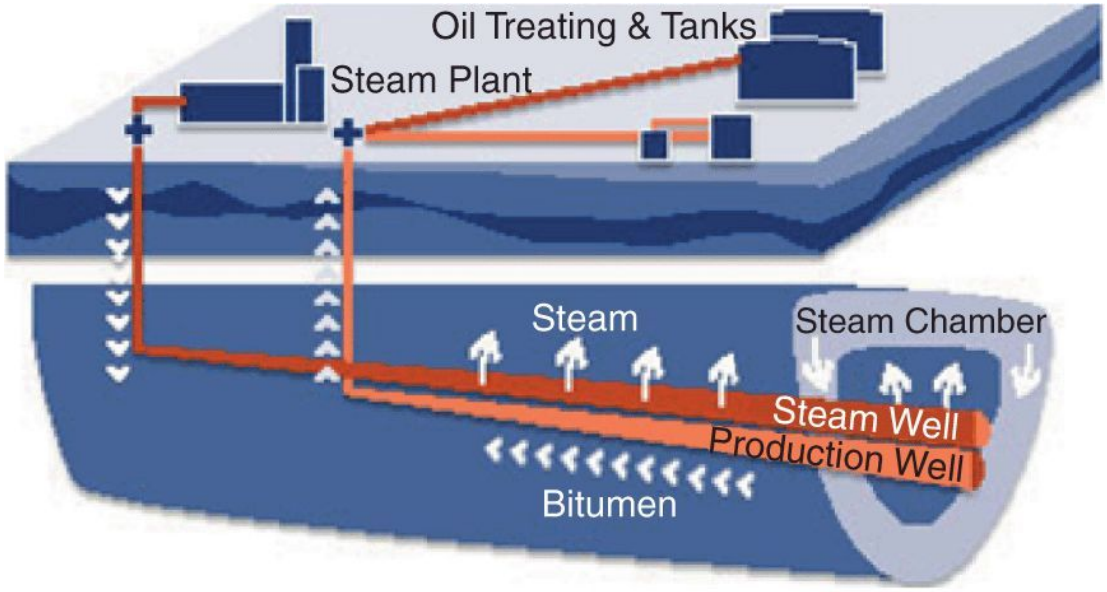

(d) Steam-assisted gravity drainage (SAGD)

Fig. 11.2–Process variations for thermal method: (a) steam soak or huff-n-puff; (b) steamdrive; (c) in-situ combustion [adapted from Prats (1982)]; (d) Steam-assisted gravity drainage (SAGD).

In-Situ Combustion. Fig. 11.2c shows a schematic of a forward in-situ combustion process. The process injects some form of

oxidant (air or pure oxygen) into the formation. The mixture then spontaneously ignites (or ignition is induced), and subsequent injection propagates a fire or burn zone through the reservoir. The fire zone is only a meter or so wide, but it generates very high temperatures. These temperatures vaporize connate water and a portion of the crude, both of which are responsible for some oil displacement. The vaporized connate water forms a steam zone ahead of the burn front, which operates very much like a steamdrive. The vaporized oil consists mainly of light components that form a miscible displacement. The reaction products of high-temperature combustion can also form an in-situ carbon dioxide (CO_2) flood. In-situ combustion processes are sometimes called high-pressure air injection (HPAI).

Steam-Assisted Gravity Drainage (SAGD) (Butler 1982). Fig. 11.2d shows a schematic of the SAGD process. This process is like both steam soak and steamdrive in that heat, carried through steam, is the recovering fluid. However, SAGD is unlike the previous two in several important respects:

- SAGD uses horizontal rather than vertical wells.
- The horizontal wells are in injector/producer pairs that are closely spaced.

Both items make SAGD different from any other thermal method, and indeed different from any other process covered in this text. SAGD is a singular example of the use of a combination of technologies (in this case, steam injection and horizontal wells) to recover oil.

Closely spaced injectors and producers (they are usually on the order of 10 m apart in SAGD) would be anathema to the other EOR processes discussed here because such close well spacing would result in early breakthrough and extensive bypassing of oil. The key to the success of SAGD is that the main recovery mechanism is buoyancy (because of density differences) rather than viscous driving forces. You will recall from Chapter 5 that in 1D flow, the

competition between buoyancy and viscous forces is expressed through a gravity number as

$$N_g^0 = \frac{k_v k_{r2}^0 \Delta\rho g}{\mu_2 u}.$$

Buoyancy is promoted when this number is large, or when u is small and/or k_V is large. A low velocity is ensured by the length of the wells (often exceeding 10,000 ft), which accumulates the very low velocities, resulting in flow. The process works best when k_V is large.

For most cases, viscosity reduction is by far the most important cause of additional oil recovery by thermal methods, but other mechanisms can also be important [e.g., distillation, miscible displacement, thermal expansion, wettability changes, cracking, and reduced oil/water interfacial tension (IFT)]. The relative importance of each mechanism depends on the oil being displaced and the process. Cracking is relatively unimportant in steam processes with their relatively low temperatures, but it is quite important during in-situ combustion. Thermal expansion and distillation become more important as the API° of the crude decreases.

Another class of thermal processes seeks to introduce heat through a reservoir using electromagnetic energy (Karanikas 2012). **Fig. 11.3** illustrates one of these processes. Although heat is introduced into the reservoir here, steam plays a minor role, and in fact can be deleterious because boiling water is a source of heat loss.

The in-situ conversion (ISC) process is different in other ways. In ISC, the intent is not so much to decrease viscosity as it is to convert the hydrocarbon chemically from a highly viscous material (tar sands and bitumen are the usual targets here) with a high carbon-to-hydrogen ratio to a much more malleable (and valuable) product with a low carbon-to-hydrogen ratio. The process resembles a subsurface refinery in which high-quality product (e.g., kerosene) is produced instead of crude. Viscous crudes form as a result of several

degradation mechanisms occurring over a long time. ISC intends to reverse this process over a short time period through heating.

In Fig. 11.3, energy is injected into a reservoir through a series of closely spaced resistive-heater wells. The combined effect of these closely spaced vertical wells is to accumulate energy over large volumes of a reservoir so that thermal cracking can occur. Other ways to introduce energy into a reservoir include resistive heating between subsurface anodes and cathodes, inductive heating, use of a heat-transfer fluid, and antennas (Carrizales 2010; Callaroti 2002).

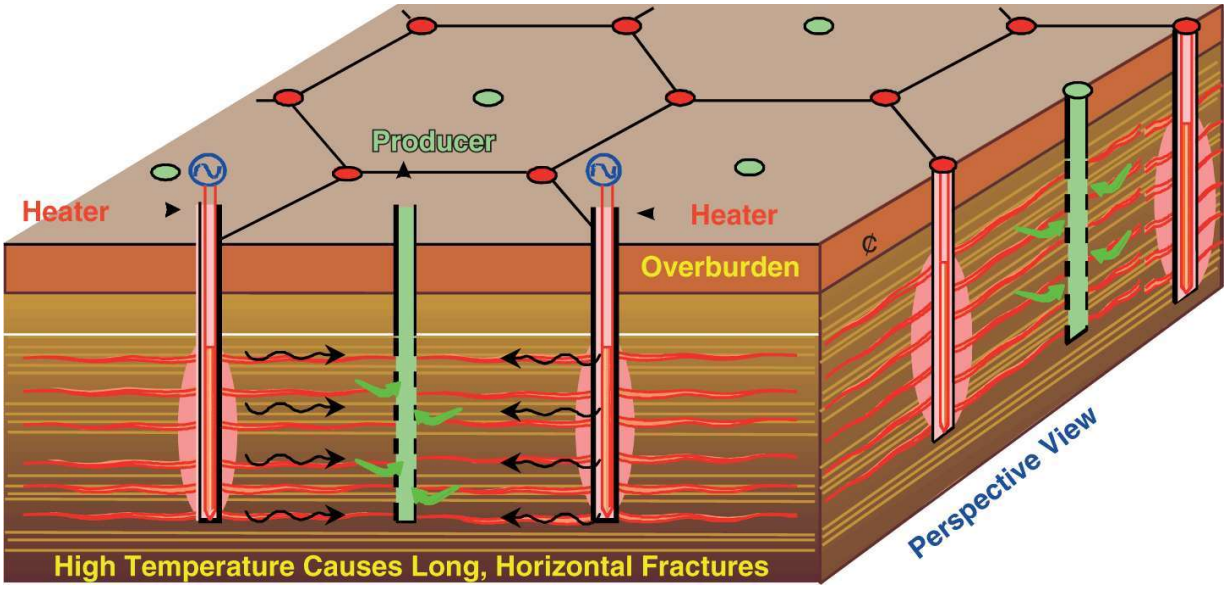

Fig. 11.3—Schematic of the in-situ conversion (ISC) process (Karanikas 2012).

11.2 Physical Properties

Elucidating the mechanisms of thermal methods begins with understanding the thermodynamic and transport properties of water and crude. We review these properties and their temperature dependence in this section. The most important water properties for this treatment are the steam/water phase envelope, steam quality, and latent heat of vaporization. For crudes, the most important property is the temperature dependence of viscosity.

11.2.1 Water Properties. The temperature rises in a thermal flood because additional energy is introduced or generated in the

reservoir. In both cases, water plays a central role. The following paragraphs review water properties; you will notice parallels to the generic treatment of phase behavior in Chapter 4.

Fig. 11.4 shows the vapor pressure of water from subatmospheric pressure to its critical point. Remember that the vapor pressure is the value of pressure (or temperature) at which a pure component (here water) changes phase (here, liquid to vapor) at a fixed value of temperature (pressure). The figure also shows the operating range for several successful steamdrives; operating pressures tend to be lower than for chemical methods and much lower than for solvent methods. Thermal methods are intrinsically low-pressure processes. As we will see in the following, the properties of saturated water are important to the efficiency of steam methods, and, therefore, the diagram also shows the range of temperatures—320–660°F (433–622 K)—for these methods.

Fig. 11.5 shows the pressure-specific volume diagram for water. The saturated vapor curve on the right of the envelope shows that steam density is much lower than saturated liquid density except very near the critical point. This figure contains lines indicating steam quality, a property discussed later.

This energy content of water is well approximated by the enthalpy. **Fig. 11.6** shows a pressure/enthalpy diagram for water. This diagram is analogous to the pressure/composition diagrams discussed in Section 4.1, with enthalpy being the composition variable. Fig. 11.6 illustrates several important landmarks.

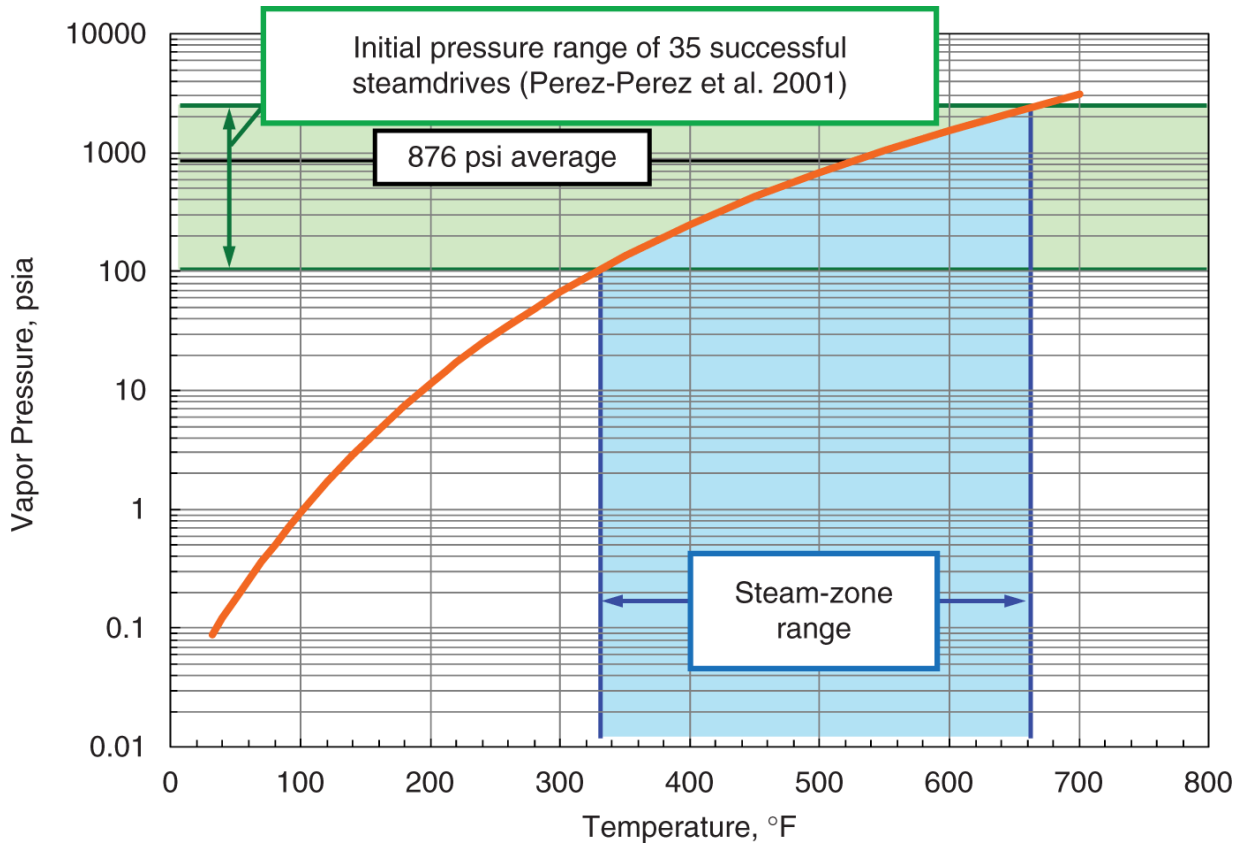

Fig. 11.4—Vapor-pressure diagram of water.

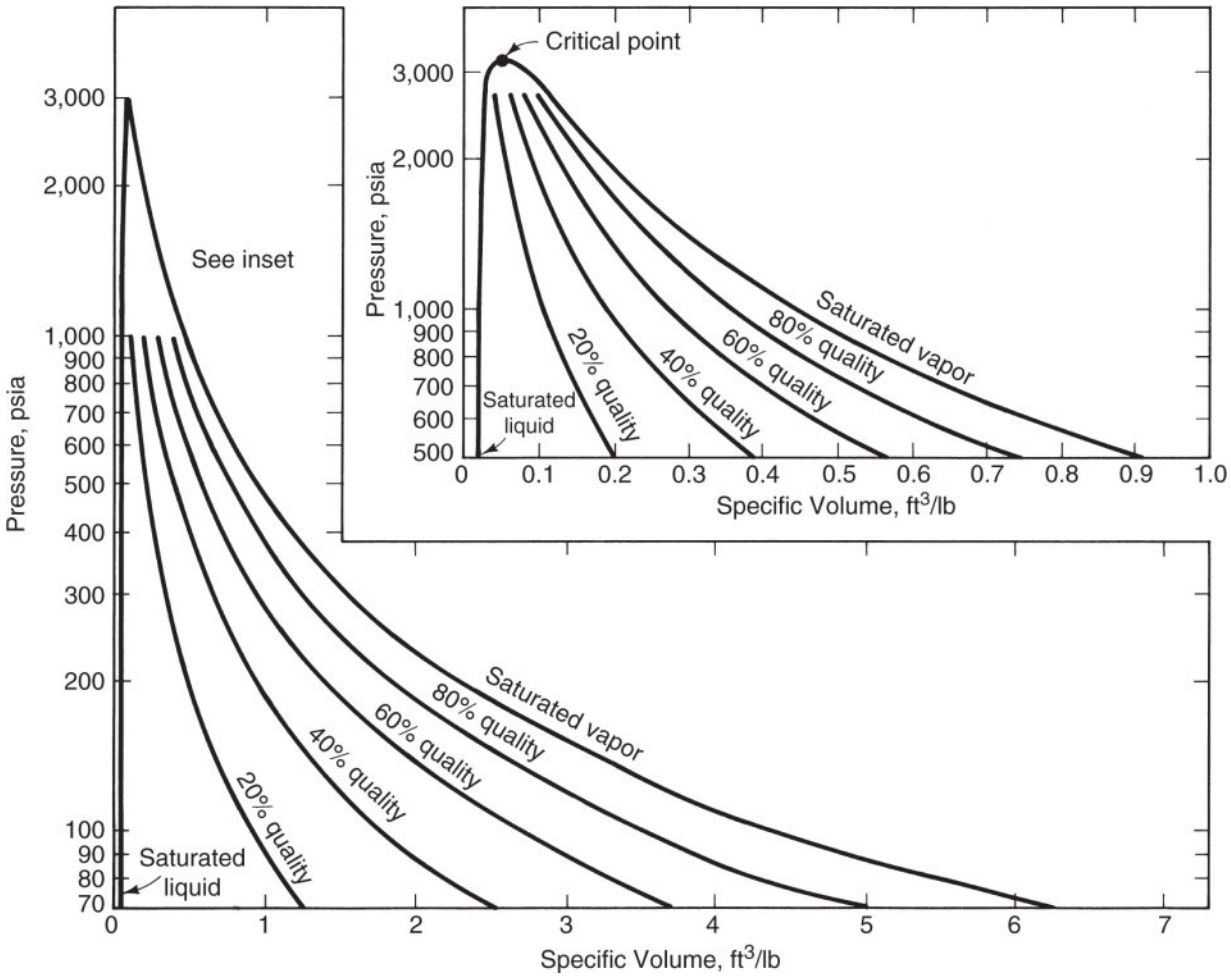

Fig. 11.5—Pressure vs. specific-volume diagram for water (Bleakley 1965).

1. Two-phase envelope. The envelope defines the region of two-phase behavior, as does the envelope on the pressure/molar volume diagram in Fig. 4.2. The left boundary is the bubblepoint curve, and the right boundary is the dewpoint curve. To the left and right of the envelope are the supercooled liquid and superheated vapor (steam) regions, respectively. Within the two-phase region, temperature depends on pressure according to Fig. 11.4. These are *saturated* temperature and pressure, respectively.
2. Steam quality. Steam quality y is the amount of the total vapor, by weight, expressed as a fraction (or a percentage) of the mass of liquid plus vapor,

$$y = \frac{\rho_3 S_3}{\rho_1 S_1 + \rho_3 S_3}. \quad (11.1)$$

Quality is normally reported as a percentage, but, like fluid saturation (the *S* in Eq. 11.1), is always used in calculations as a fraction. The quality lines within the two-phase envelope represent the relative amount of the total mass that is steam. Lines of constant temperature (only one is illustrated) in Fig. 11.6 fall steeply in the liquid region, are constant across the two-phase envelope, and then fall steeply again in the steam region.

3. Saturated liquid. A liquid is *saturated* if it exists at the temperature and pressure at which steam can be generated. The saturated-liquid curve represents 0% steam quality.
4. Saturated vapor. Saturated vapor is water at the temperature and pressure at which exactly 100% of the water present has been converted to a vapor.
   Both phases in the two-phase region are saturated.
5. Latent heat. Latent heat of vaporization L_V is the quantity of heat added to a given mass of saturated water (0% quality steam) to convert it to saturated vapor (100% quality steam) at constant temperature. The heat is *latent* because the temperature of the system does not change as the liquid is converted to vapor. On an enthalpy/pressure diagram, latent heat is the difference in the *x*-coordinates between the dewpoint and bubblepoint curves in Fig. 11.5 at a particular pressure. The latent heat vanishes at the critical point of water, 3206.2 psia and 705.4°F (21.8 MPa and 647 K). The location of the critical pressure is important in steam processes. We will show in Example 11.3 that the velocity of a steam front slows at high pressure because latent heat vanishes.
6. Sensible heat. Sensible heat is the quantity of heat that must be added to a given mass of water to raise its temperature without changing its phase. This quantity is *sensible* because a thermometer in the water will sense a temperature increase as heat is added (at a constant pressure) until steam

generation begins. Sensible heat is a product of a heat capacity and a temperature difference.

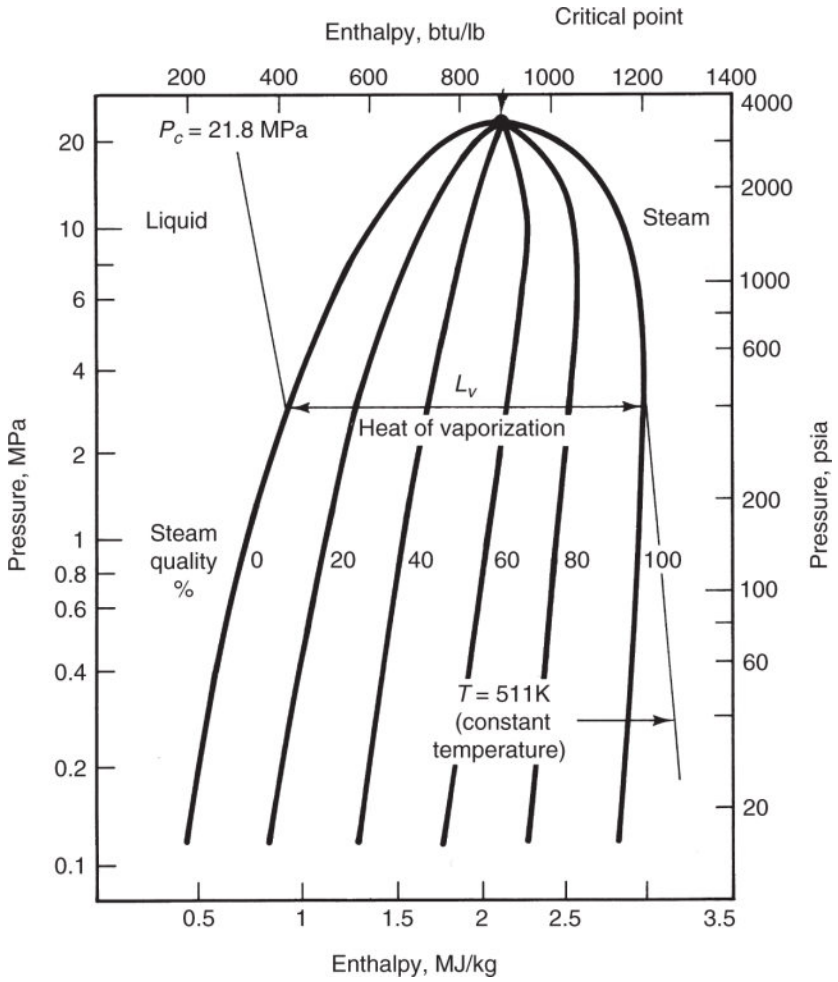

Fig. 11.6—Enthalpy vs. pressure diagram for water [adapted from Bleakley (1965)].

Thermodynamic properties, types of which are the two previous diagrams, are usually taught with temperature changing rather than pressure, as illustrated in **Fig. 11.7.** In this figure, superheated vapor is above the two-phase envelope and the supercooled region below. Constant-*T* lines within the two-phase region are vertical. As the figure illustrates, the change in enthalpy with temperature is the heat capacity,

$$C_p = \left(\frac{\partial H}{\partial T} \right)_P .$$

This can be either per mole or per mass depending on the units of H. If it is the latter, C_p is often called the *specific heat*. You can see from the plot that the heat capacity is nearly independent of both T and P (the slopes are constant) in the liquid. This is essentially the case in the vapor regions, except in the region near the critical point. We will assume constant heat capacities in much of what we do below.

The physical properties in Figs. 11.4 through 11.7 appear in steam tables (Keenan et al. 1969 and online). You should use these for precise work. Often reading information from these figures is sufficient.

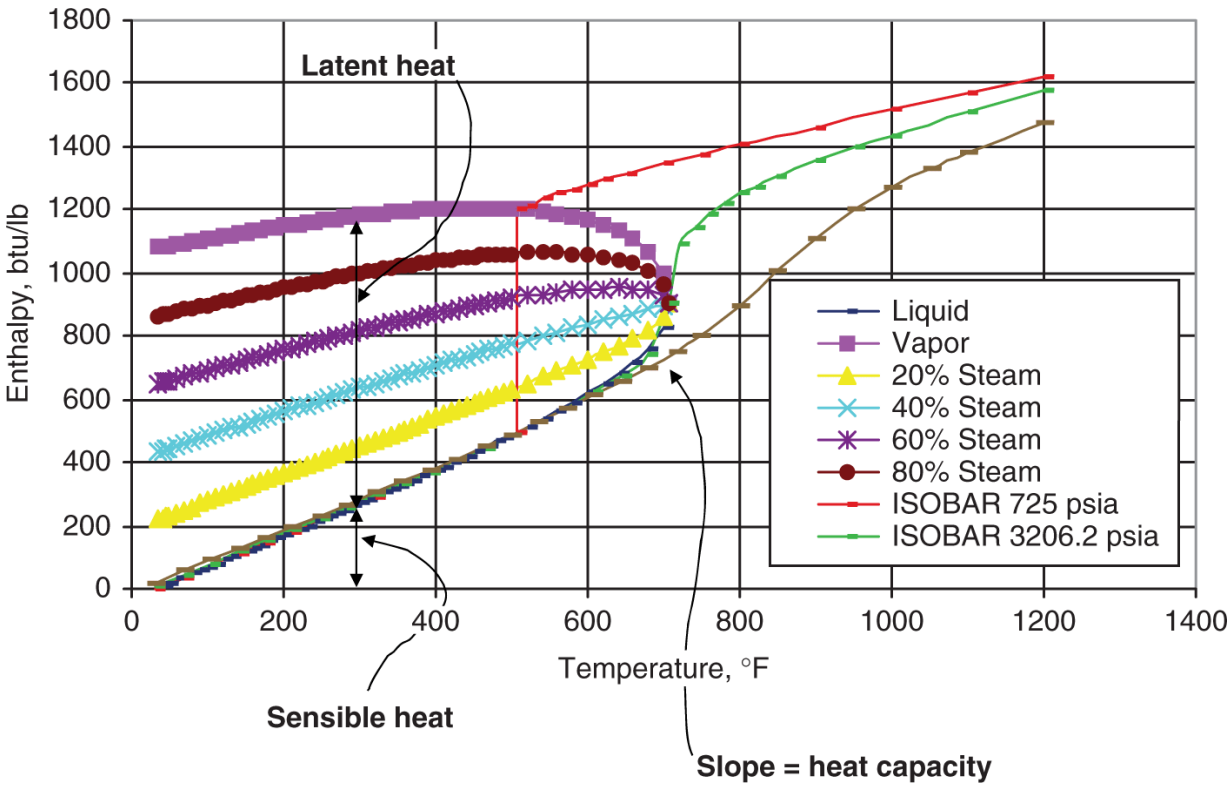

Fig. 11.7—Enthalpy-temperature diagram for water.

Example 11.1. Enthalpy Changes. Use Fig. 11.7 in the following:

a. Estimate the enthalpy content in 1 lbm of water at T = 600°F and P = 725 psia. What is the state of the fluid at this point?

The fluid is superheated vapor or steam. Directly from the graph, we have H_{13} = 1,300 Btu. Like all thermodynamic quantities, this number is relative to an arbitrary zero. Recall that the subscript 3 means vapor phase here.

b. Relative to the enthalpy of saturated water at the same T, how much of this heat is sensible and how much is latent?

Also from the graph, the enthalpies of saturated liquid (sl) and saturated vapor (sv) are [illegible], so that the enthalpy change from the conditions of Part (a) is [illegible], of which [illegible] is latent heat and the remainder, [illegible], is sensible heat. Note that the pressure had to be increased substantially to condense the fluid.

c. If the enthalpy of the fluid is H_1 = 900 Btu, what is the steam quality? From Fig. 11.6, y = 55% quality steam. Remember that all the quantities discussed here are at equilibrium.

One of the disadvantages of these graphical representations is that it is difficult to show enthalpy variations with both T and P. Farouq Ali (1974) has fitted approximate analytical expressions to water properties **(Table 11.1).**

TABLE 11.1—THERMAL PROPERTIES OF WATER [ADAPTED FROM FAROUQ ALI (1974)]

English, P [=] psia				SI, P [=] MPa				
Quantity x	a	b	Limit psia	Quantity x	a	b	Limit MPa	Percent error
Saturation temperature (°F)	115.1	0.225	300	Saturation temperature –256 (K)	197	0.225	2.04	1
Sensible heat (Btu/lbm)	91	0.257	1,000	Sensible heat (MJ/kg)	0.796	0.257	6.80	0.3
Latent heat (Btu/lbm)	1,318	–0.0877	1,000	Latent heat (MJ/kg)	1.874	–0.0877	6.80	1.9
Saturated steam enthalpy (Btu/lbm)	1,119	0.0127	100	Saturated steam enthalpy (MJ/kg)	2.626	0.0127	2.04	0.3
Saturated steam specific volume (ft^3/lbm)	363.9	–0.959	1,000	Saturated steam specific volume (m^3/kg)	0.19	–0.959	6.80	1.2

Note: $x = aP^b$.

Example 11.2. Table Comparisons. The expressions in Table 11.1 are very handy, and, therefore, it is of interest to see how well these

equations predict the actual properties. We will use the same conditions as in Example 11.1. The pressure P = 725 psi is well outside the limit of the saturation temperature and steam enthalpy in Table 11.1.

a. Estimate the saturation temperature. From the table (using English units), $T_s = aP^b = 115.1(725\ \text{psi})^{0.225} = 507°\text{F}$ compared to T = 510°F from Fig. 11.7.
b. Estimate the latent heat of vaporization. From Table 11.1, $L_v = aP^b = 1{,}318(725\ \text{psi})^{-0.0877} = 740\frac{\text{Btu}}{\text{lb}_\text{m}}$, compared to $690\frac{\text{Btu}}{\text{lb}_\text{m}}$.
c. Estimate the saturated steam enthalpy. Again, $H_{11}^{sv} = aP^b = 1{,}119(725\ \text{psi})^{0.012} = 1{,}211\frac{\text{Btu}}{\text{lb}_\text{m}}$, compared to $1{,}190\frac{\text{Btu}}{\text{lb}_\text{m}}$.
d. Estimate the saturated-steam specific volume. $v_1^{sv} = aP^b = 363.9(725\ \text{psi})^{-0.959} = 0.657\frac{\text{ft}^3}{\text{lb}_\text{m}}$, compared to $0.69\frac{\text{ft}^3}{\text{lb}_\text{m}}$ from Fig. 11.4.

Even when outside the recommended ranges, the accuracy of Table 11.1 is sufficient for most engineering purposes.

11.2.2 Crude-Oil Properties. Curiously, there seems to be no universal definition for what constitutes a heavy oil. The United States Geological Survey (USGS) definitions are given below:

- *Light or conventional oil:* Crude with an API gravity >22° and a viscosity of μ_2 < 100 mPa·s.
- *Heavy oil:* Crude with an API gravity <22° and μ_2 > 100 mPa·s.
- *Extra-heavy crude*: The portion of heavy crude with API gravity <10° and μ_2 > 10,000 mPa·s.

  All the quoted viscosities are at reservoir conditions. The USGS also adds criteria on the basis of asphaltene and sulfur content (Meyer and Attanasi 2003).
- *Natural bitumen:* Also called tar or oil sands; these are extra-heavy crudes with μ_2 > 1,000,000 mPa·s.

Easily the most important crude-oil property for thermal flooding is the viscosity dependence on temperature. As for most liquids, the Andrade (1930) equation captures this dependence:

$$\mu_2 = Ae^{B/T}, \quad \text{(11.2a)}$$

where *T* is in absolute degrees. *A* and *B* are empirical parameters for which the values are determined from two viscosity measurements at different temperatures. For extrapolation or interpolation, Eq. 11.2a indicates that a semi-log plot of viscosity vs. T^{-1} should be a straight line.

If only one measurement is available, a coarse estimate of viscosity can be obtained from **Fig. 11.8**. This single-parameter correlation assumes that viscosity change is a universal function of temperature change. To use the plot, enter the vertical axis with the known viscosity (4.38 mPa·s in this case), find the *x*-axis coordinate, move to the right by the temperature increase (101.6°C), and then return to the curve. The *y*-axis reading is the desired viscosity.

Another representation that is useful in derivation work was given by Butler (1997) as

$$\frac{v_1}{v} = \left(\frac{T - T_2}{T_1 - T_2} \right)^m, \quad \text{(11.2b)}$$

where 1 and 2 are the reference conditions, usually the saturated-steam and reservoir conditions, respectively, and *v* is the kinematic viscosity.

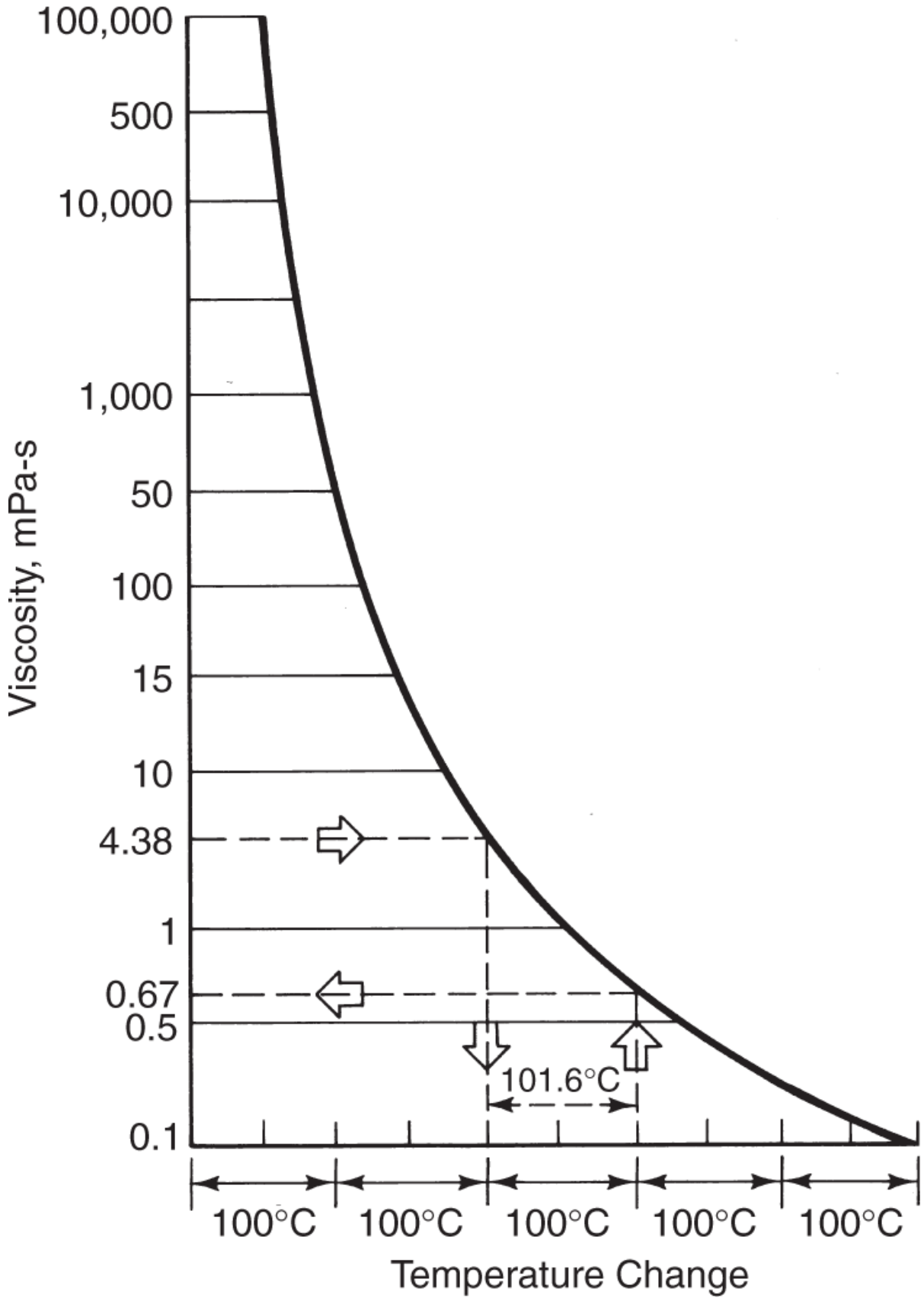
100,000
500
10,000
1,000
50
100
15
10
4.38
1
0.67
0.5
0.1
Viscosity, mPa-s
101.6°C
100°C
100°C
100°C
100°C
100°C
Temperature Change

Fig. 11.8—Single-parameter viscosity correlation (Lewis and Squires 1934).

Several other crude-oil properties, such as specific heat, volumetric heat capacity, and thermal conductivity, are functions of temperature. Empirical equations to predict these properties include the Gambill (1957) equation for specific heat,

$$C_{p2} = \frac{0.7 + 0.0032T}{\rho_2^{0.5}}, \qquad (11.2c)$$

where C_{p2} is in kJ/kg·K, T in K, and ρ_2 in g/cm^3, and the thermal conductivity (Maxwell 1950) is

$$k_{T2} = 0.135 - 2.5 \times 10^{-5} T. \qquad (11.3)$$

k_{T2} in this equation has units of kJ/m-h-K. Eq. 11.3 is based on correlations for heavy crude fractions. These estimates are generally accurate to within 5%. For more details on these correlations, see the original references.

Eqs. 11.2 and 11.3 make it possible to estimate the *thermal diffusion coefficient*,

$$K_{T2} = \frac{k_{T2}}{\rho_2 C_{p2}}, \qquad (11.4)$$

for crudes. This quantity has units of m^2/s, as do the dispersion coefficients in Eq. 2.57.

11.2.3 Solid Properties. The total thermal conductivity of an unconsolidated sand-filled medium with a single phase *j* is

$$k_{Tt} = 0.0149 - 0.0216\phi + 8.33 \times 10^{-7} k - 10^{-4}\left(\frac{D_{90}}{D_{10}}\right) + 7.77 D_{50} + 4.188 k_{Tj} + 0.0507 k_{Ts}. \qquad (11.5)$$

The parameters in this equation have their usual meanings, except that D_{10} and D_{90} are particle diameters smaller than 10 and 90% of the total sample by weight. The units on the total, fluid *j*, and solid

(k_{Tt}, k_{Tj}, k_{Ts}) thermal conductivities are J/m-s-K, the permeability k is in μm^2, and the median grain size D_{50} is in mm.

For fluid-filled consolidated sandstones, the analogous relation is

$$\frac{k_{Tt}}{k_{Td}} = 1 + 0.299\left[\left(\frac{k_{Tj}}{k_{Ta}}\right)^{0.33} - 1\right] + 4.57\left(\frac{\phi}{1-\phi}\frac{k_{Tj}}{k_{Td}}\right)^{0.482}\left(\frac{\rho}{\rho_s}\right)^{-4.30}, \quad (11.6)$$

where the subscripts a and d refer to air and dry rock. ρ is the density of the liquid-saturated rock. The thermal conductivities in Eqs. 11.5 and 11.6 are determined at a reference temperature of 293 K; they are rather weak functions of temperature, but corrections are given in Somerton (1973).

The volumetric heat capacity appears in the energy balances for thermal processes. It is defined for all phases, including the solid, as

$$M_{Tj} = \rho_j C_{pj}, \quad j = 1, \ldots, N_P, s. \quad (11.7)$$

We have encountered this quantity before in Eq. 2.83, which defined a total volumetric heat capacity.

Table 11.2 gives representative values of density, specific heat, thermal conductivity, and thermal diffusion coefficient for selected media. These values are appropriate for rough estimates of the rock-fluid thermal properties or for comparison to more refined estimates from Eqs. 11.5 through 11.7. The heat capacity of the solid phase varies relatively little with the type of solid, but the thermal conductivity can vary by a factor of two (compare the values for limestone and siltstone). The origin of the phrase, “heat can go where fluids cannot”, derives from the latter statement. The spatial variability of most nonthermal properties, permeability in particular, is far greater than this.

TABLE 11.2—DENSITY, SPECIFIC HEAT, THERMAL CONDUCTIVITY, AND THERMAL DIFFUSION COEFFICIENT OF SELECTED ROCKS [ADAPTED FROM FAROUQ ALI (1974)]

Rock	Bulk Density (g/cm^3)	Specific heat (kJ/kg-K)	Thermal conductivity (J/s-m-K)	Thermal diffusion coefficient (mm^2/s)
Dry				
Sandstone	2.08	0.729	0.831	0.55
Silty sand	1.90	0.801	(0.66)	(0.43)
Siltstone	1.92	0.809	0.649	0.42
Shale	2.32	0.761	0.989	0.56
Limestone	2.19	0.801	1.611	0.92
Fine sand	1.63	0.726	0.593	0.50
Coarse sand	1.74	0.726	0.528	0.42
Water-saturated				
Sandstone	2.27	0.999	2.610	1.15
Silty sand	2.11	1.142	(2.50)	(1.04)
Siltstone	2.11	1.094	(2.50)	(1.08)
Shale	2.38	0.844	1.600	0.79
Limestone	2.38	1.055	3.360	1.34
Fine sand	2.02	1.344	2.607	0.96
Coarse sand	2.08	1.249	2.910	1.12

Note: Values in parentheses are estimated.

Example 11.3. Heat Losses to Rock and Water. Later sections deal with various forms of heat losses, but we can introduce the largest source of heat loss now.

The total internal energy term in Eq. 2.3-1 is

$$\rho\hat{U} = \phi\sum_{j=1}^{N_P}\rho_j S_j \hat{U}_j + \left(1-\phi\right)\rho_s \hat{U}_s.$$

Away from the critical point of water, internal energies and enthalpies are nearly equal, and therefore the preceding equation becomes

$$\rho\hat{H} = \phi\left(\rho_1 S_1 \hat{H}_1 + \rho_2 S_2 \hat{H}_2\right) + \left(1-\phi\right)\rho_s \hat{H}_s.$$

We will work the hot-water case here in which the medium (the solid, subscript s) of porosity ϕ contains only water (i = 1) and oil (i = 2). You can tackle the steam case in Exercise 11.2.

Now, the fraction of heat that resides in the crude is

$$F_{\text{Heat}} = \frac{\phi\rho_2 S_2 \hat{H}_2}{\phi\left(\rho_1 S_1 \hat{H}_1 + \rho_2 S_2 \hat{H}_2\right) + \left(1-\phi\right)\rho_s \hat{H}_s}.$$

Because there is no steam, the preceding equation can be written as

$$F_{\text{Heat}} = \frac{\phi\rho_2 S_2 C_{p2}\left(T - T_{\text{ref}}\right)}{\phi\left[\rho_1 S_1 C_{p1}\left(T - T_{\text{ref}}\right) + \rho_2 S_2 C_{p2}\left(T - T_{\text{ref}}\right)\right] + \left(1-\phi\right)\rho_s C_{ps}\left(T - T_{\text{ref}}\right)},$$

where we have used the heat capacities discussed previously (assumed independent of T) and T_{ref} is a reference temperature. Using the volumetric heat capacities from Eq. 2.83, this becomes

$$F_{\text{Heat}} = \frac{\phi S_2 M_{T2}}{\phi\left(S_1 M_{T1} + S_2 M_{T2}\right) + \left(1-\phi\right) M_{Ts}}.$$

This ratio is mainly a function of the oil saturation S_2 and the porosity ϕ. Using typical values for the heat capacities (M_{T1} = 3.97 MJ/m^3·K, M_{T2} = 1.78 MJ/m^3·K, and M_{Ts} = 2.17 MJ/m^3·K) yields the following values.

F_{Heat}	$\phi = 0.2$	$\phi = 0.3$
$S_1 = 0.2$	0.16	0.23
$S_1 = 0.5$	0.09	0.14

For a high-porosity, high-S_2 media, more than 20% of the heat resides in the oil. This value falls to less than 10% for tertiary floods in a low-porosity reservoir. These percentages also suggest guidelines for the best use of thermal methods: they are most

efficient in high-porosity reservoirs (where there is less rock to heat up) undergoing secondary flooding.

Considering the success of thermal methods, such small percentages of heat going into the crude are remarkable. The success of thermal methods, where so little of the heat actually resides in the oil (recall that we have not yet accounted for losses to the wellbore and adjacent strata), must be the result of the effectiveness of this method in reducing oil viscosity (Fig. 11.1).

11.3 Fractional Flow in Thermal Displacements

11.3.1 Propagation of Thermal Fronts. Noncombustion heat fronts can propagate in three ways: as hot water, as saturated steam, or as a noncondensable gas. Each has a characteristic velocity of propagation.

Let Fluid 3 displace Fluid 1 in a 1D medium with constant cross-sectional area. There are no other fluids in the medium. As always, Fluid 1 is cold water, but Fluid 3 can be hot water, noncondensable gas, or saturated steam. Fluid 3 has a higher temperature (T^+) than Fluid 1 (T^-), and in all cases, the displacement takes place without mixing. This means that neither the miscibility (or lack thereof) of the displacement nor its stability is at issue. We further assume that conduction is negligible (this eliminates heat losses to adjacent media), that displacement takes place at constant pressure, that the reference temperature for all enthalpies is T^- (that is, $H_{i1}=0$), and finally, that all thermal properties are independent of temperature. These assumptions are the extension of the fractional-flow assumptions presented originally in Chapter 5 for thermal floods.

The equations describing this displacement are the 1D versions of the mass and energy balances, Eqs. 2.11 and 2.36. These equations are hyperbolic and reducible with the above assumptions, and, therefore, we expect the methods introduced in several previous chapters to apply here also (see Section 5.6). Under these restrictions, energy and mass waves move at the same velocity. We

can express the front velocity as a multiple of the cold-water velocity u_1/ϕ.

On the basis of Eq. 5.41b, the front velocity is

$$v = \frac{1}{\phi}\left(\frac{\rho_3 u_3 - \rho_1 u_1}{\rho_3 - \rho_1}\right), \quad (11.8)$$

and on the basis of a shock velocity derived from the conservation of energy, the same velocity is

$$v = \frac{1}{\phi}\frac{\rho_3 u_3 H_3}{\rho_3 H_3 + \left(\frac{1-\phi}{\phi}\right)\rho_s H_s}. \quad (11.9)$$

The velocities in both equations are dimensional. Eq. 11.9 neglects all forms of energy other than thermal and assumes that enthalpy is equal to internal energy. $H_s = C_{ps}(T^+ - T^-) = C_{ps}\Delta T$ is the specific enthalpy of the solid. Three special cases follow from Eqs. 11.8 and 11.9.

Fluid 3 is Hot Water. In this case, $\rho_3 = \rho_1$, $H_s = C_{ps}\Delta T$, and Eq. 11.9 becomes

$$v_{HW} = \frac{1}{1 + \frac{1-\phi}{\phi}\frac{M_{Ts}}{M_{T3}}}, \quad (11.10)$$

where v_{HW} is the specific velocity of the front, normalized by $\frac{u_3}{\phi}$, the water flux. Eq. 11.10 has used the definition (Eq. 11.83) of volumetric heat capacity and Eq. 11.39, which for this case, gives $u_3 = u_1$, so that

$$v_{HW} = \frac{1}{1 + D_{HW}}, \quad (11.11)$$

where

$$D_{HW} = \left(\frac{1-\phi}{\phi} \right) \frac{M_{Ts}}{M_{T1}} \quad \text{(11.12)}$$

is the retardation factor for the thermal front. Eq. 11.11 is a combination of the mass and energy balances. The velocity in Eq. 11.11 is independent of the temperature difference. For this case of incompressible flow, the heat fronts propagate more slowly than the tracer fronts, $v_{HW} = 1$. This slower propagation occurs because the thermal mass of the solid forces D_{HW} tends to be positive in much the same way as do the retardation factors for polymer and surfactant/polymer flooding in Eqs. 8.28a and 9.14.

Fluid 3 is Steam of Quality y. Here, we have $H_3 = C_{p1}\Delta T + yL_V$, where L_V is the latent heat of vaporization. Substituted into Eq. 11.9, this gives

$$v_{SF} = \frac{u_3}{\phi} \frac{C_{p1}\Delta T + yL_v}{C_{p1}\Delta T + yL_v + \frac{1-\phi}{\phi}\frac{\rho_s C_{ps}}{\rho_3}} \quad \text{(11.13)}$$

Eliminating u_3/ϕ using Eq. 11.8 gives

$$v_{SF} = \frac{1}{1+D_{SF}}, \quad \text{(11.14)}$$

where D_{SF} is the retardation factor for the steam front,

$$D_{SF} = \frac{D_{HW}}{1+h_D}, \quad \text{(11.15)}$$

and h_D is a dimensionless latent heat,

$$h_D = \frac{yL_v}{C_{p1}\Delta T}. \quad \text{(11.16)}$$

h_D is the ratio of latent to sensible heat. Because $h_D \geq 0$, steam fronts ($\Delta T > 0$) move faster than hot-water fronts under equivalent conditions. In other words, L_V causes the front to propagate faster because it

stores heat better. Faster-moving heat fronts are more thermally efficient because the reservoir is contacted sooner and there is less time for heat losses to the under- and overburden. D_{SF} now depends on the temperature difference (through the $C_{p1}\Delta T$ term) and on pressure (through L_V). High-pressure steamfloods approach the hot-water limit because $L_V \rightarrow 0$ as the pressure approaches the critical point of water.

Example 11.4. Propagation of Thermal Fronts. Steam fronts have a larger velocity (are more efficient) than hot-water fronts for equivalent injected enthalpy, a fact that emphasizes the effect of pressure on thermal methods. Use the saturation temperature of Fig. 11.4 and the enthalpy/pressure diagram of Fig. 11.6 in this example.

We will consider two injections: saturated steam at a pressure of 2000 psia, and 50% quality steam at P = 200 psia. Both conditions have an injected enthalpy of approximately $\hat{H}_J = 620 \frac{\text{Btu}}{\text{lb}_\text{m}}$. The initial reservoir temperature is 85°F. We will use the volumetric heat capacities from the previous example and assume that the values for saturated water are the same at both pressures. From Eq. 11.12,

$$D_{HW} = \left(\frac{1-\phi}{\phi}\right)\frac{M_{Ts}}{M_{T1}} = \left(\frac{1-0.3}{0.3}\right)\left(\frac{2.17\,\frac{MJ}{\text{m}^3\text{-K}}}{3.97\,\frac{MJ}{\text{m}^3\text{-K}}}\right) = 1.28,$$

from which we can obtain $v_{HW} = \frac{1}{1+1.28} = 0.439$. This means that the hot-water front moves at less than one-half the velocity of a tracer front.

For the saturated-steam case, we must look up some values. Fig. 11.5 gives $yL_v = (0.4)(3-0.9)\frac{MJ}{\text{kg}}$. We will need the saturated-steam temperature, which from Fig. 11.4 is T_s = 38°F, for which ΔT_s = (380–82)°F = 166 K. Then

$$h_D = \frac{yL_v}{C_{p1}\Delta T} = \frac{(0.4)(2.1)\dfrac{MJ}{\text{kg}}}{\left(1\dfrac{\text{Btu}}{\text{lb}_\text{m}\text{-}^\circ\text{F}}\right)(298^\circ\text{F})}\left\{\frac{0.454\ \text{kg}}{1\ \text{lb}_\text{m}}\frac{1\ \text{Btu}}{10^{-3}\,MJ}\right\} = 3.2$$

and $D_{SF} = \frac{D_{HW}}{1+h_D} = \frac{1.28}{1+3.2} = 0.3$, which gives the final result of $v_{SF} = \frac{1}{1+D_{SF}} = \frac{1}{1+0.3} = 0.77$. The value is twice that of a hot-water velocity, but still slower than a tracer velocity. This ordering persists over the entire pressure range up to the critical point; even the magnitude of the velocities is relatively insensitive to pressure.

In both cases, the input enthalpy was the same; it is the presence of the latent heat that causes steam to be more efficient. All steam-based processes operate more efficiently at low pressure because latent heat is larger.

The preceding equations give a way to confirm what was implicitly assumed earlier: that a steam front is self-sharpening. Let us start by combining Eqs. 11.14 through 11.16:

$$v_{SF} = \frac{1}{1+D_{SF}} = \frac{1}{1+\dfrac{D_{HW}}{1+h_D}} = \frac{1}{1+\dfrac{D_{HW}}{1+\dfrac{yL_v}{C_{p1}\Delta T}}}.$$

For a displacement of saturated water (y = 0) by 100% quality steam (y = 1), the range of velocities is

$$v_{SF}\Big|_{y=0} = \frac{1}{1+D_{HW}}$$

for saturated water and

$$v_{SF}\Big|_{y=1} = \frac{1}{1+\dfrac{D_{HW}}{1+\dfrac{L_v}{C_{p1}\Delta T}}}$$

for saturated steam. Therefore, $v_{SF}\big|_{y=0} < v_{SF}\big|_{y=1}$, and the front is a shock because the larger steam qualities move faster than the smaller qualities. The converse would, of course, be true for saturated water displacing saturated steam. That the steam front is a shock accounts for much of the success of steam drives.

Fluid 3 is a Noncondensable Gas. This case is similar to the hot-water case except that $H_3 = C_{p3}\,\Delta T$. A similar procedure to the above yields

$$v_G = \frac{1}{1+D_G}, \quad (11.17)$$

where the retardation factor is now

$$D_G = \left(\frac{1-\phi}{\phi}\right)\frac{M_{Ts}}{M_{T3}}. \quad (11.18)$$

Because $\rho_3 C_{p3}$ << $\rho_1 C_{p1}$, D_G is much greater than D_{HW}. Hence, heated gasfloods propagate the most slowly of the three cases.

11.3.2 Flow With Oil. In the next few sections, we will analyze some simple thermal displacements using fractional-flow theory. The basic governing equations are the strong forms of conservation of water,

$$\frac{\partial\left(\rho_1 S_1 + \rho_3 S_3\right)}{\partial t_D} + \frac{\partial\left(\rho_1 f_1 + \rho_3 f_3\right)}{\partial x_D} = 0, \quad (11.19a)$$

conservation of oil,

$$\frac{\partial\left(\rho_2 S_2\right)}{\partial t_D}+\frac{\partial\left(\rho_2 f_2\right)}{\partial x_D}=0, \quad \text{(11.19b)}$$

and conservation of energy,

$$\frac{\partial\left[\rho_1 S_1 H_1+\rho_2 S_2 H_2+\rho_3 S_3 H_3+\frac{(1-\phi)}{\phi}\rho_s S_s H_s\right]}{\partial t_D}+\frac{\partial\left(\rho_1 f_1 H_1+\rho_2 f_2 H_2+\rho_3 f_3 H_3\right)}{\partial x_D}=0. \quad \text{(11.19c)}$$

The mass balances are from the basic 1D fractional-flow equation (Eq. 2.53)–with water in a second phase 3–and the energy balance equation (Eq. 2.64). Of course, to write these, we have made some fairly restrictive assumptions that deserve special discussion when applied to thermal flooding.

Writing the equations in terms of fractional flow rather than flux (with f_j instead of u_j) means that we have invoked the fractional-flow assumptions. The portion of the fractional-flow assumptions least likely to apply in general is that of incompressible fluids and rock. Oil and water (hot or cold) can generally be assumed to be incompressible without great error, but steam is highly compressible. Aside from consistency with the other parts of this book and the attendant simplifications, there is no compelling reason for assuming steam to be incompressible. [For a treatment that does not assume incompressible fluids and solids, see Shutler and Boberg (1972); Aydelotte and Pope (1983).]

However, pressure gradients in steam zones are usually low, so that the densities therein can be considered approximately constant. Of course, assuming an incompressible solid means that there can be no oil production because of pore compression. The no-dissipation part of the fractional-flow assumptions now includes thermal conductivity, which is absent from Eq. 11.19c.

The equations further assume that there is no solubility of oil in water and no oil vaporization. We neglect all forms of energy except thermal energy, and we assume that internal energies are equal to enthalpies. Finally, we solve Eq. 11.19c by assuming no lateral heat loss. These assumptions mean that we can use the conventional

definitions of dimensionless time and position (Eq. 5.9) and the fractional-flow methods to solve for $S_1(x_D, t_D)$ and $T(x_D, t_D)$.

11.3.3 Hot Waterfloods. For this case, $S_3 = 0$, and the assumption of incompressible fluids and solids is good. With this, Eq. 11.19a is the only independent material balance; its strong form becomes

$$\frac{\partial S_1}{\partial t_D} + \frac{\partial f_1}{\partial x_D} = 0, \qquad (11.20a)$$

which has the saturation velocity

$$v_{S_1} = \left(\frac{\partial f_1}{\partial S_1} \right)_T \qquad (11.20b)$$

Similarly, writing the energy Eq. 2.80 in a fractional-flow form yields

$$\left(M_{T1} S_1 + M_{T2} S_2 + \frac{1-\phi}{\phi} M_{Ts} \right) \frac{\partial T}{\partial t_D} + \left(M_{T1} f_1 + M_{T2} f_2 \right) \frac{\partial T}{\partial x_D} = 0. \qquad (11.21a)$$

We have also used the mass-balance equations for water and oil to eliminate saturation derivatives. Eq. 11.20b implies a velocity for the temperature change,

$$v_T = \frac{M_{T1} f_1 + M_{T2} f_2}{M_{T1} S_1 + M_{T2} S_2 + \frac{(1-\phi)}{\phi} M_{Ts}} \qquad (11.21b)$$

v_T is a function of T only through the temperature dependence of f_j. This temperature dependence is much weaker than the dependence of μ_2 on T. Therefore, the temperature wave is a shock in hot-water displacements.

The velocities in Eqs. 11.20b and 11.21b are set equal, which yields

$$\frac{df_1}{dS_1} = \frac{f_1 + \dfrac{M_{T2}}{M_{T1} - M_{T2}}}{S_1 + \dfrac{M_{T2} + \dfrac{(1-\phi)}{\phi} M_{Ts}}{M_{T1} - M_{T2}}} \qquad (11.22)$$

on eliminating $S_2 = 1 - S_1$ and $f_2 = 1 - f_1$. Eq. 11.22 determines the water saturation S_1^* just behind the hot-water front using the construction suggested in **Fig. 11.9.** The construction is analogous to that in Fig. 8.15 for polymer flooding except that the straight material-balance line does not begin from a point on the *x*-axis. This feature, which is caused by the difference between water and oil volumetric heat capacities in Eq. 11.22, arises because water is convecting heat to the thermal front, while oil is convecting heat away from it. By our assumptions, convection is the only form of heat transfer occurring in this displacement.

The rear of the oil bank must propagate at the same velocity; hence, the extension of the material-balance line to the cold-oil fractional-flow curve gives the oil-bank saturation. The leading edge of the cold oil bank follows from the by now usual secant construction shown in Fig. 11.9.

11.3.4 Steam Displacements. We anticipate that in the absence of lateral heat loss, a steam front will propagate faster than a hot-water front (Example 11.3) and that there can be no condensation. With heat losses, some condensation can occur, but we save this discussion for the later treatment of heat losses. Behind the steam front, temperature must be constant because, by assumption, pressure is constant (pressure gradients being negligible). Hence, the entire left side of the energy balance becomes

$$\frac{\partial(\rho_3 S_3)}{\partial t_D} + \frac{\partial(\rho_3 f_3)}{\partial x_D} = 0 \qquad (11.23)$$

in one dimension. From Eqs. 11.19a, 11.19b, and 11.23, we see that the mass of each phase is conserved in the steam zone. However,

this is exactly the same problem that was solved in Section 5.7, where we considered the flow of water, gas, and oil as immiscible phases. There we constructed the composition-path diagram (Fig. 5.21), which illustrated the transition from an initial condition *I* to an injected condition *J* in two waves.

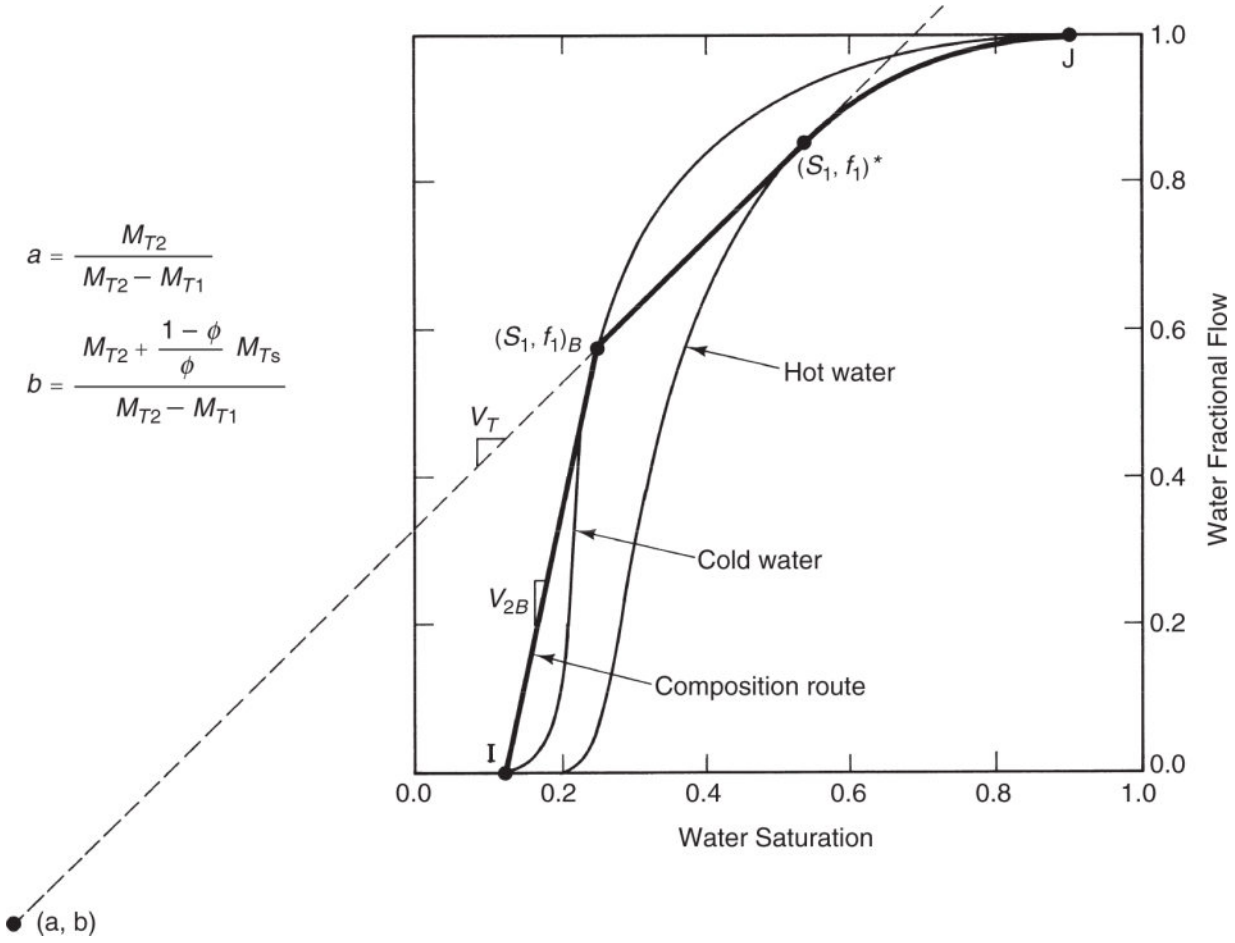

Fig. 11.9—Graphical construction of hot waterflood solution.

Although the solution presented in Fig. 5.21 is the same as the solution to a propagating steam front, they differ in one important respect: the initial condition *I* in the current problem is no longer given because this is the condition immediately behind (upstream of) the steam front. To find condition *I*, we must resort to applying the coherence condition across the steam front.

The integral coherence condition for the steam front, written in terms of oil and water amounts, is

$$\frac{\rho_1\left(f_1H_1\right)^+ + \rho_2\left(f_2H_2\right)^+ + \rho_3\left(f_3H_3\right)^+}{\underbrace{\rho_1\left(S_1H_1\right)^+ + \rho_2\left(S_2H_2\right)^+ + \rho_3\left(S_3H_3\right)^+ + \frac{(1-\phi)}{\phi}\rho_sH_s^+}_{\text{(energy)}}} = \frac{\rho_1f_1^+ + \rho_3f_3^+ - \rho_1f_1^-}{\underbrace{\rho_1S_1^+ + \rho_3S_3^+ - \rho_1S_1^-}_{\text{(water)}}} = \frac{f_2^+ - f_2^-}{\underbrace{S_2^+ - S_2^-}_{\text{(oil)}}}, \quad \ldots (11.24)$$

where the + and – represent conditions immediately upstream (the "injected" condition) and downstream of the front. No negative term appears in the energy equation because the reference temperature for enthalpy is T^- by assumption. We can simplify Eq. 11.24 by letting $H_3 = H_1 + L_V$ and $H_j = C_{pj}T$ (for j = 1 and 2). This yields

$$\frac{\left(M_{T1}f_1^+ + M_{T2}f_2^+ + M_{T3}f_3^+\right)T^+ + \rho_3L_vf_3^+}{\left(M_{T1}S_1^+ + M_{T2}S_2^+ + M_{T3}S_3^+ + M_{Ts}\right)T^+ + \rho_3L_vS_3^+} = \frac{\rho_3 + f_1^+\left(\rho_1 - \rho_3\right) - \rho_3f_2^+ - \rho_1f_1^-}{\rho_3 + S_1^+\left(\rho_1 - \rho_3\right) - \rho_3S_2^+ - \rho_1S_1^-}$$

$$= \frac{f_2^+ - f_2^-}{S_2^+ - S_2^-}. \quad \ldots (11.25)$$

Normally, the steam-zone temperature T^+ is known, leaving ten unknowns (f_j^+ and S_j^+ for $j = 1, 2, 3$, and [illegible]) in the two equations (Eq. 11.25). There are five independent relations between fractional flow and saturation—three for the upstream side and two for the downstream side—and, of course, the S_j and f_j on both sides must sum to unity, adding another two equations. We are left with an indeterminate system because there are nine total equations in ten unknowns.

One way around this problem is to invoke additional assumptions regarding the upstream conditions (Shutler and Boberg 1972). An example of this would be to let $f_j^+ = 0$. The most rigorous method would be to derive additional jump conditions by restoring the dissipative terms and solving the profile in a moving coordinate system, the so-called traveling wave problem (Bryant et al. 1986; Lake et al. 2002. Once the upstream conditions (+) have been determined, the solution proceeds, as in Section 5.7.

11.4 Heat Losses From Equipment and Wellbores

Example 11.2 showed that heat losses to rock and water easily represent the most significant source of heat loss in thermal

methods. Although preventing this is beyond our reach (except for judicious selection of thermal candidates), minimizing heat losses from equipment and wellbores and to adjacent strata *is* within our power.

11.4.1 Equipment Losses. Heat is lost from surface equipment such as pipes, fittings, valves, and boilers. Such equipment is routinely insulated, so that losses are small, except under extreme circumstances. Most heat-transfer books give procedures for detailed calculation from surface lines. **Table 11.3** gives approximate heat losses that are adequate for most designs.

11.4.2 Wellbore Losses. Heat losses from the wellbore, on the other hand, can cause a sizable energy debit if the reservoir is deep. We devote the remainder of this section to estimating wellbore-fluid temperature and quality and the rate of heat lost at a given depth. Versions of this calculation occur in production of hot fluid below aquifers and permafrost. The treatment here is for injectors, where estimates of heat loss are important to the efficiency of thermal methods.

TABLE 11.3—TYPICAL VALUES OF HEAT LOSSES FROM SURFACE PIPING

Insulation	Conditions	Heat Loss, Btu/h-ft² Surface Area for Inside Temperatures of: 200°F	400°F	600°F	800°F
Bare metal pipe	Still air, 0°F	540*	1560	3,120	–
	Still air, 100°F	210	990	2,250	–
	10-mph wind, 0°F	1,010	2,540	4,680	–
	10-mph wind, 100°F	440	1,710	3,500	–
	40-mph wind, 0°F	1,620	4,120	7,440	–
	40-mph wind, 100°F	700	2,760	5,650	–
		Heat Loss, Btu/h-ft of Linear Length of Pipe at Temperatures of:			
Magnesium pipe insulation, air temperature 80°F	Standard on 3-in. pipe	50**	150	270	440
	Standard on 6-in. pipe	77	232	417	620
	1½ in. on 3-in. pipe	40	115	207	330
	1½ in. on 6-in. pipe	64	186	335	497
	3 in. on 3-in. pipe	24	75	135	200
	3 in. on 6-in. pipe	40	116	207	322

*1 Btu/h·ft² ≅ 3.0 J/m²·s.

**1 Btu/h·ft = 0.91 J/m·s.

Estimating heat losses from a wellbore provides an excellent extended example of the application of heat-transfer theory and approximate solutions. The approach consists of three segments: steady-state heat transfer through the drillhole region, transient heat conduction in the earth adjacent to the well, and an overall heat balance on the fluid in the wellbore itself. With appropriate assumptions, each problem can be solved separately and then merged to give the final result. Combining steady-state, transient, and overall balances, as we are about to do, is a *quasisteady-state* approximation. The basic equations for strong- and weak-form energy conservation are Eqs. 2.36 and 2.92, respectively. Steady state exists when the time derivatives are zero.

11.4.3 Estimating the Overall Heat-Transfer Coefficient. Estimates of heat-transfer rate through an element of height Δz in the drillhole region can be obtained from the following equation:

$$\Delta\dot{Q} = 2\pi R_{to} U_T \left(T_f - T_d\right) \Delta z, \qquad (11.26)$$

where $\Delta\dot{Q}$ is the heat-transfer rate (energy units divided by time) through a section of a vertical wellbore Δz in height having an outer tubing radius of R_{to}. U_T is the overall heat-transfer coefficient based on the outer surface of the tubing. Using Eq. 11.26 requires an estimate of U_T.

Heat transfer through the drillhole region involves several different resistances between the fluid flowing in the tubing and the formation. Starting with the formation and moving inward, these are a cement zone, casing, annulus, tubing insulation, the tubing itself, and the flowing fluid. **Fig. 11.10** shows a schematic of the temperature profile and definitions of symbols. Eq. 11.26 is expressed in terms of the temperature difference between the fluid T_f and the temperature at the drillhole radius T_d.

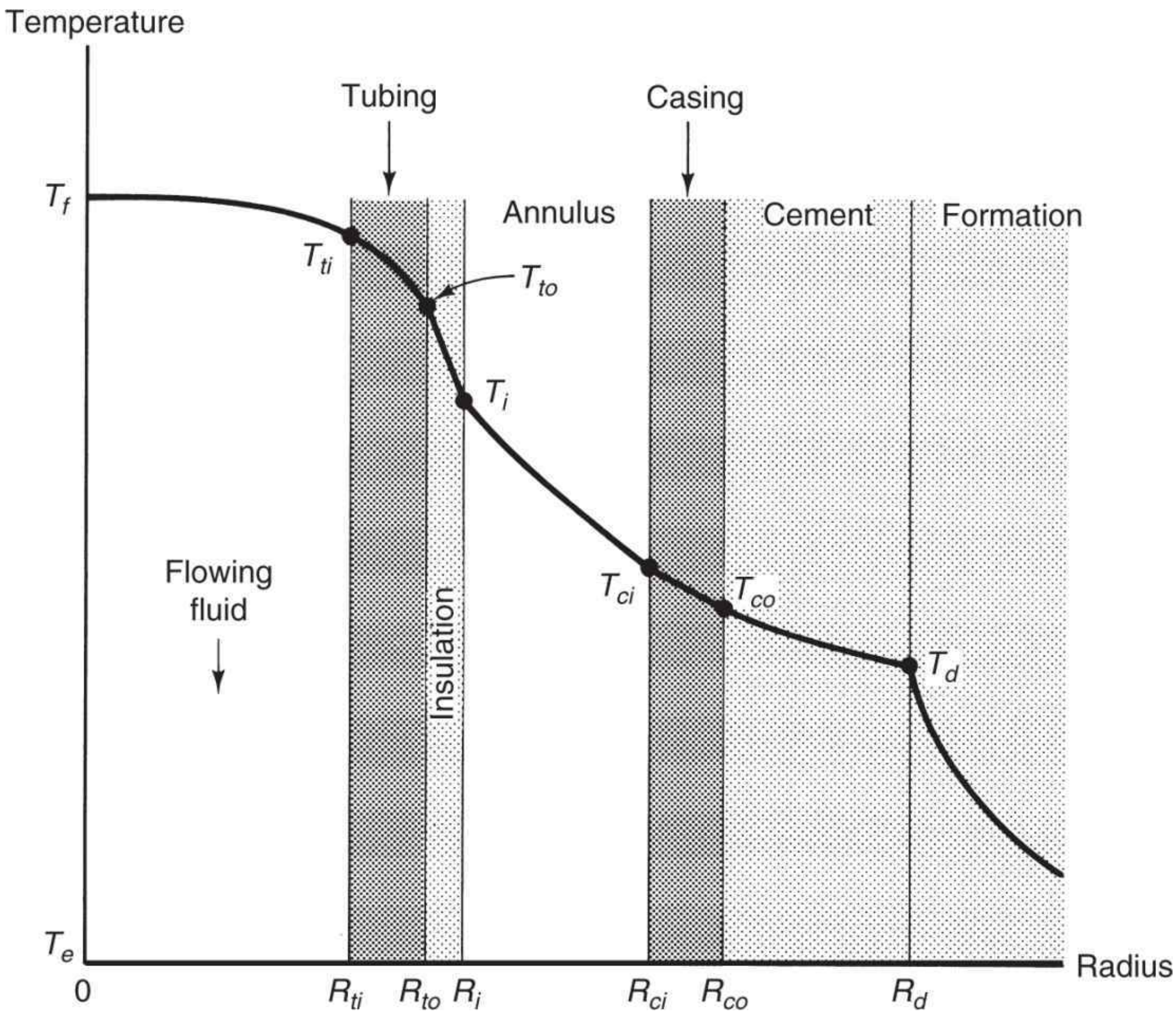

Fig. 11.10—Schematic-temperature profile in a drillhole [adapted from Willhite (1967)].

Following Willhite (1967), we assume radial symmetry in the drillhole, no heat transfer in the *z*-direction, and temperature-independent thermal conductivities. Because the drillhole region occupies a much smaller volume than the formation, it is reasonable to assume that temperature transients here decay much faster than in the formation. Therefore, we can assume that a steady-state energy balance applies in the tubing, insulation, casing, and cement:

$$\frac{d}{dr}\left(rq_c\right)=0, \qquad (11.27)$$

where q_c is the radial component of the conductive heat flux $\vec{q}_c$ in Eq. 2.33, heat transfer here being solely by conduction. Because the radius-heat flux product is a constant, the heat-transfer rate over height z is also a constant:

$$\Delta\dot{Q} = 2\pi\Delta z q_c = -2\pi r k_T \frac{dT}{dr}\Delta z. \quad \text{(11.28)}$$

Eq. 11.28 can be integrated for the temperature differences between the inside and outside of each region:

$$T_{ti} - T_{to} = \frac{\Delta\dot{Q}\ln\left(\frac{R_{to}}{R_{ti}}\right)}{2\pi k_{Tt}\Delta z} \text{ (tubing)} \quad \text{(11.29a)}$$

$$T_{to} - T_i = \frac{\Delta\dot{Q}\ln\left(\frac{R_i}{R_{to}}\right)}{2\pi k_{Ti}\Delta z} \text{ (insulation)} \quad \text{(11.29b)}$$

$$T_{ci} - T_{co} = \frac{\Delta\dot{Q}\ln\left(\frac{R_{co}}{R_{ci}}\right)}{2\pi k_{Tc}\Delta z} \text{ (casing)} \quad \text{(11.29c)}$$

$$T_{co} - T_d = \frac{\Delta\dot{Q}\ln\left(\frac{R_d}{R_{co}}\right)}{2\pi k_{T\text{cem}}\Delta z} \text{ (cement).} \quad \text{(11.29d)}$$

k_{Tt}, k_{Ti}, k_{Tc} and k_{Tcem} in Eq. 11.29a are the thermal conductivities of the tubing, insulation, casing, and cement, respectively.

Neither the fluid in the tubing nor the fluid in the annulus transfers heat strictly by conduction; hence, they must be treated separately. Let the heat-transfer rates through these regions be expressed as

$$T_f - T_{ti} = \frac{\Delta\dot{Q}}{2\pi R_{ti}\Delta z h_{Tf}} \text{ (flowing fluid)} \quad \text{(11.30a)}$$

$$T_i - T_{ci} = \frac{\Delta\dot{Q}}{2\pi R_i\Delta z h_{Ta}} \text{ (annulus fluid)} \quad \text{(11.30b)}$$

by analogy to Eqs. 11.26. h_{Tf} and h_{Ta} are the heat-transfer coefficients of the fluids in the tubing and annulus, respectively. They can be estimated mainly through correlations, as discussed in the following.

We can sum Eqs. 11.29 and 11.30 to give the overall temperature drop,

$$T_f - T_d = \frac{\Delta \dot{Q}}{2\pi \Delta z}\left[\frac{1}{R_{ti}h_{Tf}} + \frac{\ln\left(\frac{R_{to}}{R_{ti}}\right)}{k_{Tt}} + \frac{\ln\left(\frac{R_i}{R_{to}}\right)}{k_{Ti}} + \frac{1}{R_i h_{Ta}} + \frac{\ln\left(\frac{R_{co}}{R_{ci}}\right)}{k_{Tc}} + \frac{\ln\left(\frac{R_d}{R_{co}}\right)}{k_{Tcem}}\right], \quad \ldots\ldots\ldots\ldots (11.31)$$

which, inserted into Eq. 11.26, gives the overall heat-transfer coefficient,

$$U_T^{-1} = R_{to}\left[\frac{1}{R_{ti}h_{Tf}} + \frac{\ln\left(\frac{R_{to}}{R_{ti}}\right)}{k_{Tt}} + \frac{\ln\left(\frac{R_i}{R_{to}}\right)}{k_{Ti}} + \frac{1}{R_i h_{Ta}} + \frac{\ln\left(\frac{R_{co}}{R_{ci}}\right)}{k_{Tc}} + \frac{\ln\left(\frac{R_d}{R_{co}}\right)}{k_{Tcem}}\right]. \quad \ldots\ldots\ldots\ldots\ldots (11.32)$$

This equation expresses the total conductance between the fluid and the formation as a sum of series resistances each weighted by geometrical factors. If any one of the zones in Fig. 11.8 is absent (inner and outer radii equal), that term will be absent in Eq. 11.32. Moreover, if the thermal conductivity of a component is high, as is usually true with the tubing and casing, the corresponding term in Eq. 11.32 will be small. Many times, in fact, a single term will dominate the overall heat-transfer coefficient (as might occur in insulated tubing where k_{Ti} is small). Using Eq. 11.32 requires estimates of h_{Tf} and h_{Ta}.

11.4.4 Heat-Transfer Coefficient in Tubing and Annulus. The major difficulty in using Eq. 11.32 is estimating h_{Tf} and h_{Ta} because the other terms are constant. Heat transfer from a flowing fluid is by conduction and convection, and if the flow rate is large, heat is dissipated by viscous heating. **Fig. 11.11a** shows schematic velocity

and temperature profiles. Theoretical arguments (Bird et al. 2002) suggest that h_{Tf} correlates as the following dimensionless equation:

$$N_{Nu} = f\left(N_{\mathrm{Pr}}, N_{\mathrm{Re}}, N_{Br}\right) \quad (11.33)$$

for tubes with large length-to-diameter ratios. The dimensionless groups in Eq. 11.33 are

$$\text{Nusselt number} = \frac{R_{ti} h_{Tf}}{k_{Tf}} = N_{\mathrm{Nu}}, \quad (11.34a)$$

$$\text{Prandtl number} = \frac{C_{pf} \mu_f}{k_{Tf}} = N_{\mathrm{Pr}}, \quad (11.34b)$$

$$\text{Reynolds number} = \frac{2\rho_f \bar{v} R_{ti}}{\mu_f} = N_{\mathrm{Re}}, \quad (11.34c)$$

$$\text{Brinkman number} = \frac{\mu_f v_{\max}^2}{k_{Tf}(T_f - T_{ti})} = N_{\mathrm{Br}}, \quad (11.34d)$$

where the overbar in Eq. 11.34c indicates a volume average.

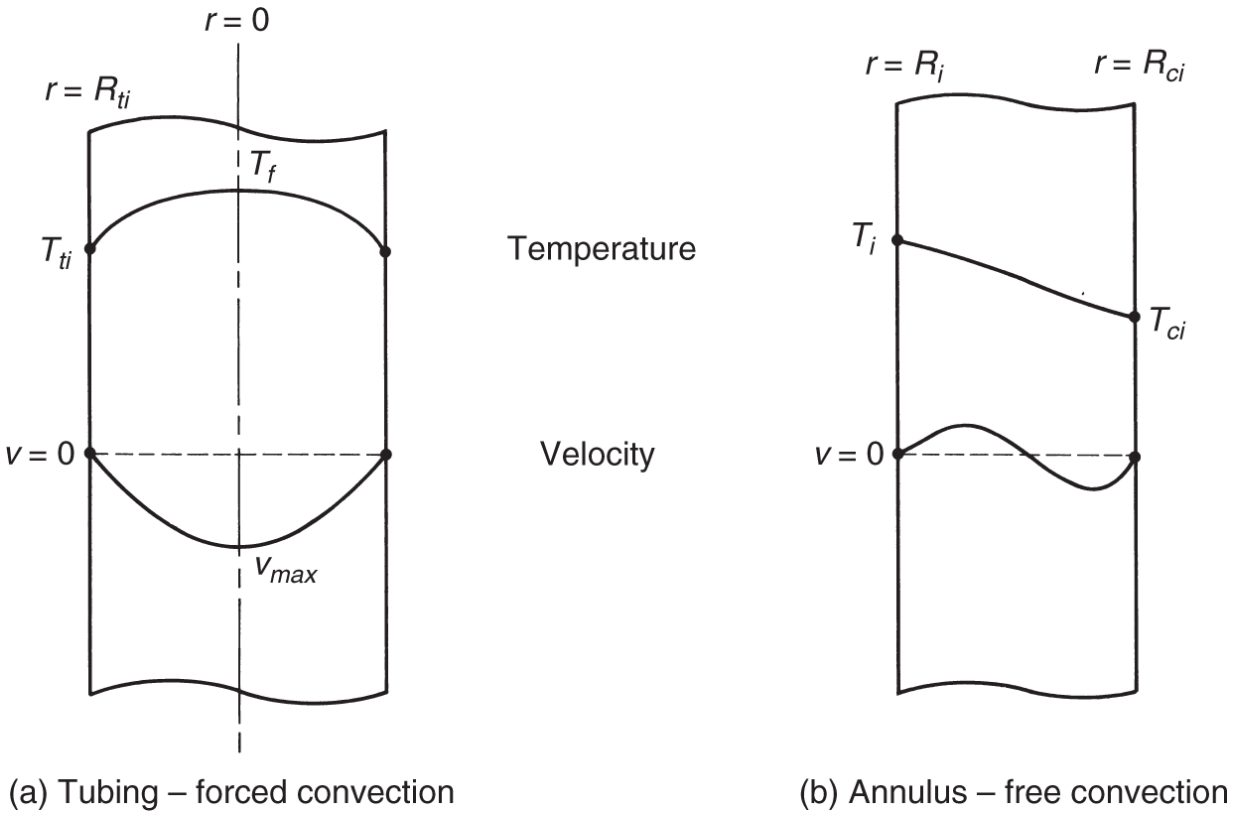

Fig. 11.11—Schematic velocity and temperature profiles in tubing and annulus [adapted from Willhite (1967)].

As their naming after persons suggests, these are familiar groups in the heat-transfer literature. Each group has a physical interpretation: N_{Nu} is the ratio of total to conductive heat transfer; N_{Pr} is the ratio of convective to conductive heat transfer; N_{Re} is the ratio of inertial to viscous forces in the fluid flow; and N_{Br} is the ratio of viscous heat dissipation to conduction. Of these four, N_{Br} is the only one containing a temperature difference; however, if it is small, as it often is for liquid flows, this dependence is weak. For simple geometry, the specific form of Eq. 11.33 can be derived theoretically; in practical cases, the relationship is empirical (Bird et al. 2002). See Exercise 11.6.

Heat transfer through an annulus is even more complicated. If the annulus is sealed at both ends, there can be no bulk flow; however, the temperature difference between T_i and T_{ci} causes local density differences in the annulus fluid that cause flow. We call such flow

free convection to distinguish it from the *forced* convection in the tubing. Fig. 11.11b shows schematic velocity and temperature profiles for the annulus. Another dimensional argument suggests a relation among dimensionless groups, a particular form of which is (Willhite 1967)

$$N_{Nu} = 0.0499\left(N_{Gr} N_{\mathrm{Pr}}\right)^{1/3} N_{\mathrm{Pr}}^{0.074} \quad (11.35)$$

for flat plates with large length-to-diameter ratios. The additional group in Eq. 11.35 is the Grashof number,

$$N_{Gr} = \frac{\left(R_{ci} - R_i\right)^3 g \rho_a \beta_T \left(T_i - T_{ci}\right)}{\mu_a}, \quad (11.36)$$

which is the ratio of free convection transport to viscous forces. The parameter β_T is a thermal expansion coefficient defined as $-1/\rho_a(\partial_a/\partial T)_P$, and the subscript *a* refers to the annulus fluid. The fluid properties in N_{Nu}, N_{Pr}, and N_{Gr} are now based on the annulus fluid. The Grashof number contains a temperature difference that is usually unknown a priori; therefore, in applications, it may be necessary to solve for heat loss by trial and error.

Usually an annulus is air-filled, but on occasion, it has been evacuated. When this occurs, heat transfer is almost exclusively through radiation. Radiation is a form of heat flux independent of convection or conduction. Under some circumstances, radiation can account for a substantial fraction of heat transfer.

11.4.5 Heat Conduction in the Formation. The immense thermal mass of the earth surrounding the wellbore, only a small fraction of which is in contact with the reservoir, suggests that heat transfer here is transient. In this segment, we repeat a procedure first described by Ramey (1959) for calculating temperatures beyond the drillhole, $r > R_d$.

Let heat transfer in the formation be strictly by radial conduction. In the absence of any velocities, Eq. 2.36 becomes

$$\frac{\partial T}{\partial t} = \left(\frac{k_T}{\rho C_p} \right)_s \frac{1}{r} \frac{\partial}{\partial r} \left(r \frac{\partial T}{\partial r} \right) = \frac{K_{Ts}}{r} \frac{\partial}{\partial r} \left(r \frac{\partial T}{\partial r} \right), \quad (11.37)$$

where Eq. 2.34 has been inserted for conductive heat flux and Eq. 11.4 has been used for the thermal diffusion coefficient. Eq. 11.37 also assumes an incompressible, single-phase formation so that a change in internal energy is manifest only as a change in temperature (there is no latent heat). Once this equation has been solved for $T(t, r)$ for $r > R_d$, the heat-transfer rate follows from the spatial gradient at $r = R_d$. The following boundary and initial conditions apply to Eq. 11.37:

$$T(0, r) = T(t, \infty) = T_e. \quad (11.38a)$$

$$-k_{Ts} \left(\frac{\partial T}{\partial r} \right)_{r=R_d} = \frac{\Delta \dot{Q}}{2\pi R_d \Delta z}, \quad (11.38b)$$

where Δz is the overall height difference. The undisturbed external temperature T_e is a function of z because of the geothermal gradient

$$T_e = a_T z + T_0, \quad (11.39)$$

where a_T is usually approximately 0.18 K/km, and T_0 is the mean surface temperature. The existence of this gradient implies a constant rate of heat transfer from the Earth's core; it also suggests a z-dependency in the problem that is not explicit in the equations. The solution, therefore, will be for a particular z, but the variation with z arises only when solving the energy balance for the flowing fluid. Eq. 11.38b expresses the continuity of heat flux at $r = R_d$. Combining it with Eq. 11.26 gives the "conduction" condition,

$$-k_{Ts} \left(\frac{\partial T}{\partial r} \right)_{r=R_d} = \frac{U_T R_{to} \left(T_f - T_d \right)}{R_d}. \quad (11.40)$$

As discussed earlier, all temperatures are functions of z.

For nonzero R_d, the solution to Eqs. 11.37, 11.38, and 11.40 must be numerical (using Laplace inversion), but once it is known, the heat-transfer rate follows from Eq. 11.38b to give

$$\Delta\dot{Q} = \frac{2\pi k_{Ts}\left(T_d - T_e\right)\Delta z}{f_T\left(t_D\right)}, \quad (11.41)$$

where f_T is a function of dimensionless time t_D and formation Nusselt number,

$$t_D = \frac{K_{Ts}t}{R_d^2} \quad (11.42a)$$

$$N_{\mathrm{Nu}} = \frac{R_{to}U_T}{k_{Ts}}. \quad (11.42b)$$

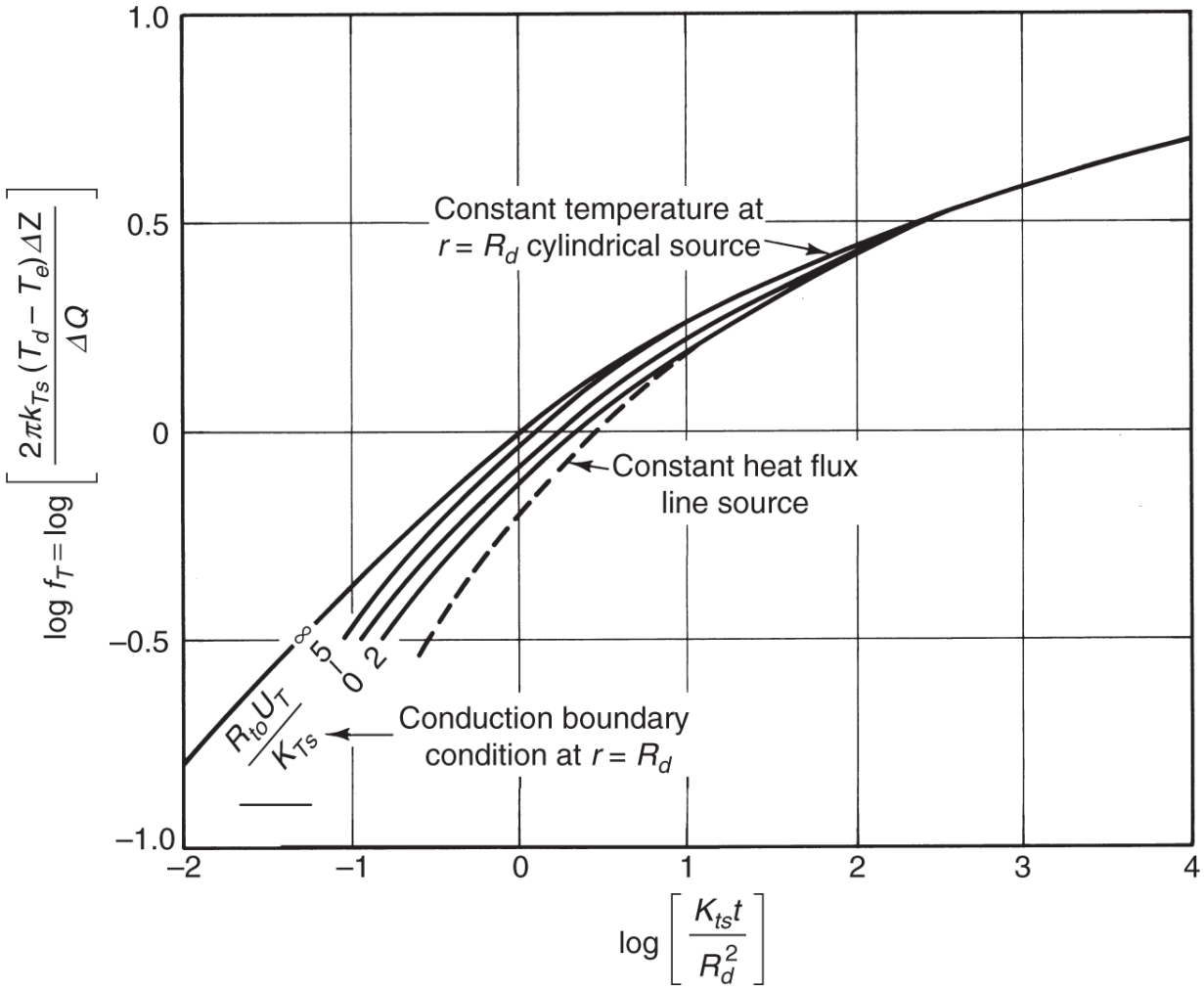

Fig. 11.12—Transient heat-transfer function (Ramey 1962).

Fig. 11.11 shows the logarithm of f_T plotted vs. the logarithm of t_D with N_{Nu} as a parameter.

Ramey (1959) gives the procedure for using these equations. Let us solve for the inner casing temperature T_{ci} and heat loss rate $\Delta\dot{Q}$ at a given depth and time. We know the radii in **Fig. 11.12**; the thermal conductivities of the tubing, insulation, casing, and cement zone; the thermal properties of the flowing fluid, the annulus fluid, and the formation; the viscosity and average velocity of the flowing fluid; and the depth z and the bulk fluid temperature T_f. The procedure is as follows:

1. Calculate T_e from Eq. 11.39 and calculate N_{Pr} and N_{Re} for the flowing fluid and N_{Pr} for the annulus fluid from Eqs. 11.34. Calculate t_D from Eq. 11.42a.
2. Assume a value for h_{Ta} and calculate U_T from Eq. 11.32, all other quantities being independent of temperature. If N_{Br} is not small, a value for h_{Tf} must be assumed also.
3. Calculate the formation Nusselt number from Eq. 11.42b and, using this and t_D, estimate f_T from Fig. 11.12. Calculate T_d from

$$T_d = \frac{T_f f_T\left(t_D\right) + \left(\dfrac{k_{Ts}}{R_{to} U_T}\right) T_e}{f_T\left(t_D\right) + \left(\dfrac{k_{Ts}}{R_{to} U_T}\right)} \quad \text{(11.43)}$$

   T_f in this equation follows from eliminating $\Delta\dot{Q}$ between Eqs. 11.26 and 11.41. We can now calculate $\Delta\dot{Q}$ from either equation.
4. With $\Delta\dot{Q}$ and T_d known, the casing temperature T_{ci} and all the others follow from successive application of Eqs. 11.29 and 11.30.

   The solution would now be complete, but the assumed value of h_{Ta} in Step 2 may be incorrect. Proceeding further requires a trial-and-error process.
5. Calculate N_{Gr} from Eq. 11.36 and use Eq. 11.35 to estimate h_{Ta}. If radiation is important, we would correct for it here.
6. Recalculate U_T from its definition (Eq. 11.32). Compare this value to that used in Step 2; repeat Steps 2 through 6 with the new value of U_T if agreement is not satisfactory. The convergence test is on U_T, a much weaker function of temperature than h_{Ta}. Convergence should be obtained in three or fewer steps.

11.4.6 Heat Loss From the Wellbore. We now focus attention on the element Δz, through which heat is passing at rate $\Delta\dot{Q}$. First, we eliminate T_d between Eqs. 11.26 and 11.41 to give

$$\Delta\dot{Q} = \frac{2\pi k_{Ts} R_{to} U_T}{k_{Ts} + R_{to} K_{Ts} f_T\left(t_D\right)}\left(T_f - T_e\right)\Delta z. \quad (11.44)$$

In what follows, we assume U_T to be constant.

If we apply the overall energy balance (Eq. 2.56) to the element Δz, we have

$$A\Delta z \frac{d}{dt}\left(\overline{\rho_f U}\right) + \Delta\dot{H} - \bar{v}\rho_f Ag\Delta z = -\Delta\dot{Q}, \quad (11.45a)$$

where we have neglected kinetic energy and mechanical work terms. Furthermore, by writing the enthalpy rate entering and leaving Δz as the product of a specific enthalpy and a constant mass flow rate $\dot{m} = \bar{v}r_{\rho f}A,$ we can obtain

$$\dot{m}\left(\Delta\overline{H} - g\Delta z\right) = -\Delta\dot{Q}. \quad (11.46b)$$

Eq. 11.46b has also dropped the time derivatives using the same quasisteady-state argument used previously for the drillhole.

The simplest heat-loss model follows from Eq. 11.41 by assuming that T_f is constant at the surface inlet temperature (this makes $\Delta\overline{H} = 0$) and integrating the resulting ordinary differential equation for dQ/dz (in the limit $\Delta z \rightarrow 0$) (Ramey 1964):

$$\dot{Q}\left(z\right) = \frac{2\pi k_{Ts} R_{to} U_T}{k_{Ts} + R_{to} U_T f_T\left(t_D\right)}\left[\left(T_f - T_0\right)z - \frac{a_T z^2}{2}\right], \quad (11.46)$$

where we have replaced T_e by Eq. 11.39 and T_d by Eq. 11.26 before integrating. This equation yields the maximum heat-loss rate up to depth z because the temperature difference between T_f and T_e is the maximum possible value. $(T_f - T_0)$ is the difference between inlet and surface temperatures.

For more general cases, let us eliminate $\Delta\dot{Q}$ between Eqs. 11.44 and 11.45b, which yields, after again taking the limit as $\Delta z \rightarrow 0$,

$$\frac{d\overline{H}}{dz} - g = -\frac{2\pi k_{Ts} R_{to} U_T \left(T_f - T_e\right)}{\dot{m}\left[k_{Ts} + R_{to} U_T f_T\left(t_D\right)\right]}. \quad \text{(11.47)}$$

Eq. 11.47 is a working equation. The sign convention is that z increases downward and $\dot{Q}$ is positive when heat is lost from the wellbore. We can invoke Eq. 11.47 for several special cases by taking different forms for the specific enthalpy.

If the fluid flowing in the tubing is an ideal gas, because single-phase steam would be at low pressure, the enthalpy is independent of pressure:

$$d\overline{H} = C_{p3} dT_f. \quad \text{(11.48a)}$$

Substituting this into Eq. 11.47,

$$\frac{dT_f}{dz} = \frac{g}{C_{p3}} - \frac{2\pi k_{Ts} R_{to} U_T \left(T_f - T_e\right)}{C_{p3}\dot{m}\left[k_{Ts} + R_{to} U_T f_T\left(t_D\right)\right]}. \quad \text{(11.48b)}$$

Eq. 11.48b will integrate to

$$T_f = a_T z + T_0 - A_T\left(a_T + \frac{g}{C_{p3}}\right) + \left[\left(T_f - T\right)_0 + A_T\left(a_T + \frac{g}{C_{p3}}\right)\right] e^{-z/A_T} \quad \text{(11.48c)}$$

for constant heat capacity, where

$$A_T\left(t_D\right) = \frac{\dot{m} C_{p3}\left[k_{Ts} + R_{to} U_T f_T\left(t_D\right)\right]}{2\pi k_{Ts} R_{to} U_T} \quad \text{(11.48d)}$$

and T_{fo} in Eq. 11.48c is the inlet surface temperature at $z = 0$. With T_f now determined as a function of depth, we can integrate Eq. 11.45b for the heat loss down to z. These two equations state that the fluid temperature and heat loss vary with depth as an exponential function

plus a linear term, the rate of change being determined by A_T, which is proportional to the mass flow rate.

If the flowing fluid is a superheated vapor at the inlet surface temperature, Eq. 11.48c will describe its temperature down to the saturation temperature. Below this point, the fluid will be a saturated two-phase mixture for some distance down in the tubing, where the fluid will condense gradually to saturated water as more heat is lost. In this case, the specific enthalpy relates to the steam quality as

$$\overline{H} = H_1^{sl} + yL_v \quad \text{(11.49a)}$$

If pressure is constant, this leads to a relatively simple differential equation in quality (Satter 1965),

$$\frac{dy}{dz} = \frac{g}{L_v} - \frac{\left(T_f - T_e\right)}{A_T}, \quad \text{(11.49b)}$$

where

$$A_T\left(t_D\right) = \frac{\dot{m}L_v\left[k_{Ts} + R_{to}U_T f\left(t_D\right)\right]}{2\pi R_{to}k_{Ts}}. \quad \text{(11.49c)}$$

Because a change in steam quality at constant pressure must take place at constant temperature, we can integrate Eq. 11.49b with T_f constant at the saturation temperature for the fluid quality in the tubing,

$$y = 1 + \left[\frac{\left(\frac{gA_T}{L_v}\right) + T_0 - T_f}{A_T}\right]z + \frac{a_T z^2}{2A_T}, \quad \text{(11.49d)}$$

where $y = 1$ at $z = 0$. The heat loss follows from Eq. 11.49a; note that a constant flowing temperature does not imply the absence of heat loss if the fluid is condensing.

Eq. 11.49d is deceiving in its simplicity. It has neglected the hydrodynamics of two-phase flow in a vertical pipe and the